# A newly identified linker protein ApcI regulates light harvesting under red light in *Synechocystis* sp. PCC 6803

Roberto Espinoza-Corral[a,d]; Tomáš Zavřel[e]; Markus Sutter[a,b,c]; Chase H. Leslie[f]; Kunwei Yang[f]; Warren F. Beck[f]; Jan Červený[e]; Cheryl A. Kerfeld[a,b,c,d*].

[a]MSU-DOE Plant Research Laboratory, Michigan State University, East Lansing, MI, 48824, USA
[b]Environmental Genomics and Systems Biology Division, Lawrence Berkeley National Laboratory, Berkeley, CA, 94720, USA
[c]Molecular Biophysics and Integrated Bioimaging Division, Lawrence Berkeley National Laboratory, Berkeley, CA, 94720, USA
[d]Department of Biochemistry and Molecular Biology, Michigan State University, East Lansing, MI, 48824, USA
[e]Department of Adaptive Biotechnologies, Global Change Research Institute of the Czech Academy of Sciences, Brno, 603 00, Czech Republic
[f]Department of Chemistry, Michigan State University, East Lansing, Michigan 48824-1322, USA

*To whom correspondence should be addressed:
Cheryl A. Kerfeld: ckerfeld@lbl.gov

**Keywords:** Phycobilisomes, Photosystem, *Synechocystis*, light harvesting

**Abbreviations**: PS: photosystem; PBS: phycobilisome; APC: allophycocyanin

**Abstract**

Phycobilisomes are versatile cyanobacterial antenna complexes that harvest light energy to drive photosynthesis. They can adapt to various light conditions, for example, dismantling under high light to prevent photo-oxidation and arranging in rows under low light to increase light harvesting efficiency. Light quality also influences phycobilisome structure and function, as observed under far-red light exposure. Here we describe a new phycobilisome linker protein ApcI (previously hypothetical protein Sll1911), expressed specifically under red light (620 nm), or upon chemically induced reduction of the plastoquinone pool. We characterized ApcI in *Synechocystis* sp. PCC 6803 using mutant strain analyses, phycobilisome binding experiments, and protein interaction studies. Deletion of *apcI* conferred high light tolerance to *Synechocystis* sp. PCC 6803 as compared to the wild type strain, exhibiting a reduction of energy transfer from phycobilisomes to the photosystems under high light. Binding experiments revealed that ApcI replaces the linker protein ApcG at the membrane-facing side of the phycobilisome core via a paralogous C-terminal motif. Additionally, the N-terminal region of ApcI was found to interact with photosystem II. Our findings highlight the importance of phycobilisome remodeling for adaptation to different light conditions. The characterization of ApcI provides new insight into the mechanisms by which cyanobacteria optimize light-harvesting in response to varying light conditions.

## Introduction

Harvesting of light energy in photosynthetic organisms is highly regulated to drive photosynthesis under diverse environmental conditions (Sanfilippo et al., 2019). In cyanobacteria, light is captured by water-soluble phycobilisomes (PBSs), which are pigment-protein complexes that transfer absorbed energy to the reaction centers of photosystems embedded in the thylakoid membrane (Gantt et al., 1968; Govindjee and Shevela, 2011). One example of antenna adaptation is the formation of rows of PBSs closely packed with photosystem II (PSII) under low light (Ho et al., 2017; Rast et al., 2019). Likewise, light quality changes trigger adaptive mechanisms to optimize photosynthesis, such as state transitions, which regulate the allocation of energy to PSII or photosystem I (PSI) to prevent saturation of the electron transport chain and the production of reactive oxygen species (Tamary et al., 2012). Other adaptive processes in cyanobacteria include proteome changes, such as the reduction of the size of antenna complexes under intense light and the expression of the Orange Carotenoid Protein for the dissipation of excess light energy captured by the PBS (Kirilovsky and Kerfeld, 2016; Zavrel et al., 2019; Kerfeld and Sutter, 2024; Srivastava et al., 2024).

PBSs harvest light energy through cyanobilins, pigments covalently bound to phycobiliproteins, which tune their spectroscopic properties (Adir et al., 2020; Beck, 2024) to ensure directionality of energy transfer from rods to the core and ultimately to the photosystems (Sil et al., 2022). The PBS from *Synechocystis* sp. PCC 6803 (hereafter referred to as *Synechocystis*) consists of a tricylindrical core surrounded by six rods forming a hemidiscoidal arrangement (Adir et al., 2020; Dominguez-Martin et al., 2022; Bryant and Gisriel, 2024; Sauer et al., 2024). Linker proteins play an important role in the PBS structure by connecting the core cylinders and attaching the rods to the core (Bryant and Canniffe, 2018; Dominguez-Martin et al., 2022; Sauer et al., 2024).

PBSs have been reported to undergo structural remodeling involving various proteins to tune light harvesting under light quality changes (Bryant and Gisriel, 2024). The recently identified cyanobacterial PBS linker, ApcG (Dominguez-Martin et al., 2022) has been shown to play a role in energy transfer from PBS to the photosystems (Espinoza-Corral

et al., 2024). An algal ApcG homolog (Lpp2) was subsequently identified in the hemiellipsoidal PBS from red alga *Porphyridium purpureum* (You et al., 2023). More recently, the ApcG ortholog from the cyanobacterium *Arthrospira* sp. FACHB439 was shown to interact with PSII through its N-terminal region. The interaction appears to be transient and unstable (Zhang et al., 2024). Likewise, in *Synechocystis,* the PBS rods containing the linker protein CpcL are able to interact with PSI, which might regulate photosynthetic activity under stress conditions, such as iron deficiency (Watanabe et al., 2014; Shimizu et al., 2023; Zheng et al., 2023). In addition, cyanobacteria express the chlorophyll binding protein IsiA in response to iron deficiency, forming rings of IsiA monomers around PSI (Guikema and Sherman, 1983; Burnap et al., 1993; Toporik et al., 2019). Under low light conditions, IsiX (homolog of IsiA) is expressed along with ApcD4 and ApcB3 which have been proposed to form antenna-like complexes interacting peripherally with PSI (Soulier et al., 2020; Soulier et al., 2022; Gisriel et al., 2023a). A unique adaptation of cyanobacterial photosynthesis is the expression of far-red light PBSs, consisting of rodless bicylindrical cores exhibiting red shifted absorbance maxima as the specific proteins expressed under these conditions tune the spectral properties of the bilins (Gisriel, 2024; Gisriel et al., 2024).

Here we identify and characterize a new PBS linker protein. We identified this protein, previously known as hypothetical protein Sll1911, through its sequence homology to the C-terminal, PBS-binding region of ApcG. We named this linker protein ApcI; ApcH was recently named in the heptacylindrical PBS from *Anthocerotibacter panamensis* (Jiang et al., 2023). While the C-terminal region of ApcI interacts with the PBS, its N-terminal region interacts with PSII, enabling energy transfer from PBS to PSII. An *apcI* deletion mutant demonstrated light tolerance to high light intensities compared to wild type (500-1000 µmol photons $m^{-2} \cdot s^{-1}$). We propose that under conditions that reduce the plastoquinone pool, ApcI can substitute for ApcG in binding to the PBS and interacts with PSII, increasing the efficiency of photosynthesis. Our results describe a new linker protein and a new mode for the remodeling of the interaction of the PBS with PSII under different environmental conditions.

## Results

### ApcI homologs contain a conserved PBS binding motif

The recently described linker protein ApcG shows a conserved C-terminal PBS binding motif that interacts with ApcA at the membrane-facing side of the PBS core (Dominguez-Martin et al., 2022). When we searched cyanobacterial proteomes with only the PBS binding motif of ApcG, we were able to identify a large number of homologs (244 in 377 proteomes that contain ApcE, see **Supplementary Table S1** and Methods for details). Interestingly, these homologs aligned well with the PBS binding motif but were very different from ApcG in the rest of their primary structure (**Figure 1A**). The homolog in *Synechocystis* corresponds to the hypothetical protein Sll1911 which we have named ApcI in accordance with precedent in the literature (Jiang et al., 2023).

Analysis of the sequence conservation among the 244 ApcI homologs revealed three discrete regions in the protein: the N-terminal region, middle region, and the PBS binding motif (**Figure 1B**). The C-terminal region of ApcI resembles the ApcG PBS binding motif in terms of its sequence (**Figure 1A**) and predicted alpha helical structure. Beyond the conserved C-terminal region, ApcG and ApcI share no significant sequence homology.

However, as the ApcG N-terminal regions interact with PSII in the thylakoid membrane (Espinoza-Corral et al., 2024), we hypothesized that the N-terminal region of ApcI could likewise interact with other complexes and tether the PBS to them. An Alphafold structure prediction (Jumper et al., 2021) suggests that the N-terminal region of ApcI is unstructured while the middle region shows secondary structure elements with a moderate confidence score (**Figure 1C**). The C-terminal FxxM motif of ApcG (also found in the PBS linker protein CpcG (Zheng et al., 2025)) which interdigitates with ApcA (Dominguez-Martin et al., 2022) is also conserved across all ApcI homologs (**Figure 1B**), suggesting that ApcI binds to a similar site in the PBS core.

A sequence search of 377 cyanobacterial genomes that contain at least one gene encoding for ApcE shows that ApcI homologs are found in 64 % of the cyanobacterial genomes (244 out of 377) in contrast to ApcG which is found in 86 % of the genomes

(325 out of 377) (**Supplementary table S1**). PBSs can be classified into different types based on the length of ApcE (Bryant and Canniffe, 2018); they can either be bicylindrical (Glazer et al., 1979), tricylindrical (Bryant et al., 1979; Zheng et al., 2021) or pentacylindrical (Glauser et al., 1992; Ducret et al., 1998). Interestingly, ApcI is more often found in PBSs with a bicylindrical or tricylindrical core (180 out of 194 and 8 out of 9 respectively) compared to pentacylindrical PBS (56 out of 174) (**Figure 1D**). In contrast, ApcG seems to be the more common PBS linker protein as it is present in the majority of the species analyzed regardless of their PBS core type (**Figure 1D**).

**Expression and physiological role of ApcI in light harvesting**

To study the role of ApcI (*sll1911* gene locus) we generated a deletion strain (Δ*apcI),* replacing its native coding sequence with a chloramphenicol resistance cassette. Using the previously characterized Δ*apcG* strain (Espinoza-Corral et al., 2024), we then generated a double mutant for both linker proteins (Δ*apcI*-Δ*apcG),* replacing the native coding sequence of *apcI* by a kanamycin resistance cassette while in the strain with the *apcG* replaced by a chloramphenicol resistance cassette (**Supp. Figure S1**). Strains were grown under different white light intensities to compare their behavior at high light intensities. The Δ*apcI* strain showed a similar phenotype to the wild type between 25 - 750 µmol photons $m^{-2} \cdot s^{-1}$ and improved light tolerance at the highest tested light intensity of 1000 µmol photons $m^{-2} \cdot s^{-1}$. On the other hand, the Δ*apcG* strain showed an increased light tolerance compared to both wild type and Δ*apcI* strains above 500 µmol photons $m^{-2} \cdot s^{-1}$. Strikingly, the double mutant strain (Δ*apcI*-Δ*apcG*) showed remarkable light tolerance in contrast to the wild type, Δ*apcI* and Δ*apcG* strains for which specific growth rates started to decrease as a consequence of photo-inhibition above 750 µmol photons $m^{-2} \cdot s^{-1}$ (**Figure 2A**). Pulse amplitude modulation fluorometry measurements showed that the maximal electron transport rate ($ETR_{max}$) decreased for wild type, Δ*apcI* and Δ*apcG* strains under high light while the double mutant maintained $ETR_{max}$ constant throughout all light intensities (**Figure 2B**). Furthermore, the double mutant showed lower $ETR_{max}$ compared to the other strains at low and middle light intensities (between 25 and 500

μmol photons $m^{-2} \cdot s^{-1}$) suggesting impaired energy transfer from PBSs to the photosystems as a consequence of the loss of both ApcG and ApcI (**Figure 2B**). Interestingly, an analysis of non-photochemical quenching (qN, a parameter to diagnose light stress) measured in strains grown under 1000 μmol photons $m^{-2} \cdot s^{-1}$ showed that wild type, Δ*apcI* and Δ*apcG* strains experienced similar levels of light stress unlike the double mutant strain where negligible qN was measured (**Figure 2C**). Whole-cell absorption spectra from all strains were similar when grown under normal conditions (i.e., 25 μmol photons $m^{-2} \cdot s^{-1}$), however mutant strains showed increased absorbance between 400 to 500 nm (**Figure 2D**). To better resolve the spectral features, we recorded low temperature absorption spectra (77K), showing a similar trend indicating carotenoid accumulation compared to wild type (**Figure 2E**).

The high light tolerance exhibited by the Δ*apcI* strain compared to wild type (**Figure 2A**) suggests that ApcI could play a role in energy transfer from PBSs to the photosystems at the thylakoid membrane. To test this, we compared low temperature fluorescence spectra (77K) from cells grown under white and red light (hereafter referring to a light source with a peak at 620 nm), exciting chlorophyll (at 430 nm) and PBS (at 590 nm) separately. Emission spectra were represented as relative values to the normalization point being either 800 nm (chlorophyll emission spectra) or 660 nm (PBS emission spectra). Chlorophyll emission spectra for cells grown under white light were indistinguishable among strains, indicating that PSII (680 nm peak) and PSI (720 nm peak) abundance was unaffected by the lack of *apcI* (**Figure 3A**). Moreover, red light grown cultures (reducing plastoquinone pool and inducing state II) (Fuente et al., 2021; Zavrel et al., 2024) showed a higher PSII fluorescence for wild type and Δ*apcI* compared to Δ*apcG* and the double mutant (Δ*apcI*-Δ*apcG*), consistent with the observed effect of ApcG on photosystem energy balance (Espinoza-Corral et al., 2024) (**Figure 3B**). Interestingly, when exciting PBSs with white or red light grown cultures, PSII and PSI showed decreased fluorescence for all mutant strains compared to the wild type strain, indicating that the lack of either linker protein reduces the energy transfer from PBSs to both photosystems (**Figure 3**). Statistical analyses after emission peak deconvolution revealed

that after exciting at 430 nm (**Supp. Figure 2**), photosystem fluorescence was not significantly different across strains, except for a reduction in PSI fluorescence in double mutant strain (**Figure 3C**). In contrast, PBS emission spectra deconvolution (**Supp. Figure 3**) for Δ*apcI* and Δ*apcI*-Δ*apcG* strains showed a significant reduction in relative fluorescence of both photosystems when excited at 590 nm under white or red light (**Figure 3D**). Interestingly, the single mutant Δ*apcG* strain showed a reduction of PSII fluorescence only in cultures grown under red light (**Figure 3D**). We tested whether $CO_2$ supplementation and the light intensity differences between white light (25 µmol photons $m^{-2} \cdot s^{-1}$, with $CO_2$ supplementation) and red light (4 µmol photons $m^{-2} \cdot s^{-1}$, without $CO_2$ supplementation) conditions contributed to chlorophyll emission spectra differences. However, cultures grown under 4 µmol photons $m^{-2} \cdot s^{-1}$ of white light (without $CO_2$ supplementation) showed spectra similar to the cells grown under 25 µmol photons $m^{-2} \cdot s^{-1}$ (**Supp. Figure S4**). Additionally, we monitored the level of PSII, PSI and PBS protein accumulation by western blots using antibodies against their respective marker proteins. Interestingly, PSII and PBS levels were stable among strains grown under white or red light, while PSI showed a reduction only in wild type strains grown under red light (**Supp. Figure S5**). Therefore, we conclude that the emission spectra differences among strains were not due to different levels of PBSs or photosystems.

Proteomic analysis indicates that ApcI expression is induced under increasing light intensities (Zavrel et al., 2019). Additionally, transcriptomic data showed higher *apcI* transcripts in red light grown cultures (Luimstra et al., 2020). Using antibodies raised against full length ApcI (**Supp. Figure S6**), we identified that ApcI expression is indeed triggered by red light exposure (4 µmol photons $m^{-2} \cdot s^{-1}$), while we could not detect ApcI in white light grown cultures (**Figure 4A**). Since red light exposure is known to trigger state II in cyanobacteria which is characterized by a highly reduced plastoquinone pool (Khorobrykh et al., 2020; Fuente et al., 2021; Zavrel et al., 2024), we hypothesized that the reduced plastoquinone pool in the thylakoid membrane is the trigger for ApcI expression. To test this, we cultivated wild type and Δ*apcI* strains under white light (25

244 µmol photons $m^{-2} \cdot s^{-1}$) in the presence of DBMIB (an inhibitor of the cytochrome $b_6f$
245 complex consequently preventing the oxidation of the plastoquinone pool) (Mao et al.,
246 2002), thus chemically creating a potential trigger for ApcI expression. In the presence of
247 DBMIB (Dibromothymoquinone), we could detect ApcI in wild type cultures grown under
248 white light (**Figure 4B**). Further, we incubated the wild type strain for one day under red
249 light in the presence or absence of DCMU (N-(3,4-dichlorophenyl)-N-dimethylurea, an
250 inhibitor of electron transport chain at PSII, to prevent the reduction of plastoquinone pool)
251 (Mao et al., 2002). Indeed, an oxidized plastoquinone pool created by DCMU precludes
252 the expression of ApcI in cultures grown under red light (**Supp. Figure S7**), confirming
253 that the plastoquinone pool redox state is likely the trigger for ApcI expression, rather than
254 the specific light quality. We then analyzed the localization of ApcI in *Synechocystis* cells
255 by comparing membrane and soluble fractions from cultures grown under red light.
256 Interestingly, ApcI was mainly found in the soluble fraction, consistent with its putative
257 interaction with the PBS, while a small portion of it remained with the membrane fraction
258 (**Figure 4C**).
259
260 **ApcI interacts with the PBS and PSII**
261 Because the C-terminal region of ApcI is similar to the PBS binding motif from ApcG (e.g.,
262 FxxM motif which interdigitates with ApcA, **Figure 1A**) (Dominguez-Martin et al., 2022),
263 we tested for the binding of ApcI to the PBS *in vitro*. Isolated PBSs from wild type and
264 double mutant Δ*apcI*-Δ*apcG* strains were incubated with purified full length ApcI (**Supp.**
265 **Figure S6A**) followed by a discontinuous sucrose gradient centrifugation to separate
266 unbound protein (located at the top of the sucrose gradient, F1) and collected the PBS
267 fraction (F2) (**Figure 5A**). Fractions containing PBSs were precipitated by trichloroacetic
268 acid (TCA) and analyzed by Western blot using ApcI specific antibodies. Interestingly,
269 ApcI was found to bind only to PBSs in the double mutant strain Δ*apcI*-Δ*apcG* (**Figure**
270 **5B**), suggesting that a wild type PBS-bound ApcG prevents the interaction of ApcI at the
271 same site. Antibodies against ApcI cross-react with ApcG, however, the two proteins can
272 be distinguished by their molecular masses (15 kDa for ApcI and 20 kDa for ApcG) (**Supp.**
273 **Figure S8**). To confirm that ApcI and ApcG bind to the same site we performed
274 competition experiments using isolated PBSs from the double mutant strain Δ*apcI*-Δ*apcG*

and the purified proteins ApcI and ApcG (**Supp. Figure S6**). When mutant PBSs (Δ*apcI*-Δ*apcG*) were incubated with a mixture of ApcI and ApcG at equimolar ratio, ApcG prevented the binding of ApcI to PBSs, supporting the hypothesis that these proteins bind to the same site in the PBS core (**Figure 5C**).

While their C-terminal regions are structurally and functionally similar, the lack of similarity between the rest of the ApcI and ApcG suggests that these proteins play different roles and interact with different partners. Low temperature fluorescence from Δ*apcI* showed impaired energy transfer to both PSI and PSII (**Figure 3**), suggesting it plays a role in the interaction between PBSs and photosystems. To identify the interaction partner of ApcI at the thylakoid membrane, we designed a truncated version of ApcI, replacing its PBS binding motif with a His tag (ApcI$^{\Delta 74\text{-}128}$-His) that allowed both purification of the protein as well as a method to pull down interaction partners (**Figure 6A**). However, incubation of ApcI$^{\Delta 74\text{-}128}$-His with solubilized thylakoids (in the presence of 1 % dodecyl-beta-D-maltoside) induced aggregation of ApcI (**Supp. Figure S9A**). We then incubated ApcI$^{\Delta 74\text{-}128}$-His with the soluble fraction from *Synechocystis* lysates and we found that the eluate from nickel beads was green (**Supp. Figure S9B**). Western blot analyses using the eluate from ApcI$^{\Delta 74\text{-}128}$-His incubated with the soluble fraction from cyanobacteria lysates showed the presence of the D1 protein of PSII (PsbA) but no detectable APC nor PSI proteins (PsaB) (**Figure 6B**). In order to confirm the interaction of ApcI with PSII, we generated a complemented strain for ApcI by replacing the native *psbA2* gene copy with the *apcI* wild type open reading frame in the background of the Δ*apcI*-Δ*apcG* strain. This strategy ensured strong expression of *apcI* under the control of the *psbA2* promoter (P*psbA2*) (Englund et al., 2016; Espinoza-Corral et al., 2024). Thylakoid complexes were separated on native gels and transferred to a membrane for the detection of ApcI using antibodies. Indeed, ApcI could be detected at the band where PSII is located (**Figure 6C**), suggesting that the N-terminal extension of ApcI binds to PSII.

## Discussion

Linker proteins play fundamental roles in regulating energy transfer between the PBS and the photosystems. Their distinct features may relate to the overall PBS architecture as

well as the environment in which they evolved. For example, the recently discovered protein ApcH acts as an anchor for the two extra core cylinders in the heptacylindrical PBS from *Anthocerotibacter panamensis* (Jiang et al., 2023). Besides the terminal emitters ApcE and ApcD that are known to participate in energy transfer to PSII and PSI, respectively (Gindt et al., 1992; Dong et al., 2009; Liu et al., 2013), recent cryogenic electron tomography structures of an algal PBS interacting with photosystems revealed additional linker proteins involved in the PBS-PS interaction (You et al., 2023). Under low light and far-red light conditions, the cyanobacterial photosynthetic apparatus undergoes major remodeling along with alterations of the PBS structure. These structural shifts include the synthesis of chlorophyll *f* and *d* in PSII and rodless bicylindrical cores composed of specific phycobiliproteins that tune the absorption of bilins to drive photosynthesis under far-red light (Ho et al., 2016; Ho et al., 2017; Herrera-Salgado et al., 2018; Gisriel et al., 2023b). In *Synechocystis*, the linker protein ApcG participates in the PBS interaction with PSII as well as in regulating energy balance between photosystems (Espinoza-Corral et al., 2024), highlighting the role of linker proteins in PBS energy transfer. ApcI is a new member of the family of PBS linker proteins and was discovered due to its PBS binding motif, which is similar to that of ApcG. The occurrence of ApcI among relatively fewer cyanobacterial species compared to ApcG suggests that ApcI is a specialized, adaptive linker protein, while ApcG is the main PBS-PSII linker under ambient conditions (**Supplementary table S1**). Indeed, *Synechocystis* proteomic data shows that under normal conditions (with a combination of red and blue photons and 25 µmol photons $m^{-2} \cdot s^{-1}$ light intensity) ApcG levels are a hundredfold more abundant compared to ApcI (Zavrel et al., 2019). Additionally, increasing light intensity during *Synechocystis* cultivation reduces ApcG accumulation along with other antenna proteins while the expression of ApcI increases (Zavrel et al., 2019), suggesting a specific role of ApcI under high light conditions. Furthermore, ApcI occurrence in cyanobacteria is more often associated with bi- and tri-cylindrincal PBSs and less often in pentacylindrical (**Figure 1D**), suggesting there may be a correlation with PBS core structure and the linker protein that interacts with the photosystems.

Cyanobacterial growth under high light conditions (from 500 to 1000 µmol photons $m^{-2} \cdot s^{-1}$ white light) is impaired as a consequence of photo-damage caused by the saturation of PSII (Nishiyama et al., 2006). However, comparison of wild type to single mutant strains Δ*apcI* and Δ*apcG* shows that the loss of function of either linker protein provides tolerance to high light conditions, with the Δ*apcG* strain exhibiting higher light tolerance compared to the Δ*apcI* strain (**Figure 2A**). Interestingly, *apcI* transcripts are more abundant under high light (Kopf et al., 2014), red light (Luimstra et al., 2020) and darkness (Saha et al., 2016) (conditions known to reduce the plastoquinone pool) (Khorobrykh et al., 2020; Fuente et al., 2021) compared to normal conditions (25 µmol photons $m^{-2} \cdot s^{-1}$ white light), which suggests an adaptive role for ApcI under these conditions. Surprisingly, the double mutant Δ*apcI*-Δ*apcG* strain displayed remarkable light tolerance highlighting the role of these linker proteins in light harvesting (**Figure 2A**). Additionally, the Δ*apcI*-Δ*apcG* strain showed slower growth rate under lower light intensities compared to single mutants and wild type (from 25 to 300 µmol photons $m^{-2} \cdot s^{-1}$ white light), consistent with the role of these linker proteins in the PBS-PS interaction (**Figure 2A**). Interestingly, the $ETR_{max}$ of the double mutant Δ*apcI*-Δ*apcG* strain did not change under higher light intensities (**Figure 2B**), which could explain why this strain exhibits light tolerance; it might not be able to saturate the electron transport rate when missing both the ApcG and the ApcI linker proteins. Absorption spectra of strains grown under normal conditions (25 µmol photons $m^{-2} \cdot s^{-1}$ white light) showed higher absorbance between 400 and 500 nm for mutant strains. Low temperature absorbance spectra measurements suggest that this increase of absorbance (especially for Δ*apcI*) is very likely to be due to carotenoids (**Figure 2D-E**). Carotenoids are known to accumulate in cyanobacteria under stress conditions (Zakar et al., 2017; Rodrigues et al., 2023), which indicates that mutant strains Δ*apcI* and Δ*apcG* might experience stress due to the lack of the connectivity between PBSs and photosystems.

The behavior of the mutant strains compared to wild type suggests that their energy transfer from PBSs to photosystems is reduced. In 77K emission spectra when exciting

chlorophyll (at 430 nm), no differences were observed between wild type and Δ*apcI* strains grown under white or red light (**Figure 3**). In contrast, Δ*apcG* and double mutant Δ*apcI*-Δ*apcG* strains showed lower PSII emission when grown under red light triggering state II (Calzadilla and Kirilovsky, 2020; Fuente et al., 2021), consistent with the role of ApcG in photosystem energy balance (Espinoza-Corral et al., 2024). On the other hand, PBS emission spectra (exciting at 590 nm) showed lower PSII and PSI fluorescence for all mutant strains compared to wild type under both white and red light (**Figure 3**), indicating that ApcI is indeed necessary for the energy transfer from PBSs to the photosystems. It is interesting that while Δ*apcG* showed differences in both chlorophyll and PBS emission spectra compared to wild type, Δ*apcI* only showed differences in PBS emission spectra, suggesting that only ApcG participates in regulating energy balance between photosystems. The expression of ApcI is shown to be triggered by a reduced plastoquinone pool, either induced by red light, or chemically (**Figure 4**). Interestingly, comparison of growth and $ETR_{max}$ under red light cultivation showed that the double mutant Δ*apcI*-Δ*apcG* strain did not show light tolerance as it does under white light cultivation. On the contrary, the highest light tolerance between the tested strains was found in Δ*apcG* (**Supp. Figure S10**). Under red light, Δ*apcI* strain performed slightly worse compared to wild type as well as to Δ*apcG*, which suggests a putative role of ApcI under light quality changes (**Supp. Figure S10**). Although ApcI expression is lower under white light compared to red light (**Figure 4**) (Jahn et al., 2018), the single mutant Δ*apcI* strain exhibits a reduction of PSII and PSI fluorescence compared to wild type under both white and red light (**Figure 3**), indicating that ApcI participates in light harvesting under both light quality conditions. Despite the more reduced plastoquinone pool triggered by red light compared to white light illumination (Fuente et al., 2021), ApcI mediated PBS-PSII interaction did not lead to a plastoquinone pool over reduction (**Supp. Figure S11**) suggesting no photo-damage occurs under the conditions tested to trigger ApcI expression. On the contrary, it seems to optimize electron transport rate on the thylakoid membrane, which helps to keep ATP/NADPH ratio stable over a wide range of light intensities (Hoper et al., 2024).

PBS binding and pulldown experiments show that ApcI and ApcG bind to PBSs in the same site (**Figure 5**), and the ApcI N-terminus (residues 1-73) binds to PSII (**Figure 6**). Furthermore, an ApcI homolog from the cyanobacterium *Synechococcus sp.* PCC 7002 (LcpA, gene A0913) was recently shown to interact with PSII (Zheng et al., 2025), consistent with ApcI pulldown experiments (**Figure 6**). Moreover, a mutant strain lacking LcpA exhibited impaired growth and reduced $O_2$ evolution under white light compared with the wild type (Zheng et al., 2025), also consistent with our findings (**Figure 2** and **3**). These results pose the question of the localization of ApcI, either attached to the PBS or at the thylakoid membrane. Localization of ApcI from strains grown under red light showed that the majority of ApcI is in the soluble fraction (**Figure 4C**). However, PBSs isolated from strains grown under red light, which induces the expression of ApcI (**Figure 4C**), did not have ApcI bound but ApcG was present (**Supp. Figure S12**). Nevertheless, the lack of ApcI still reduces the energy transfer from PBSs to photosystems as shown in 77K emission spectra (**Figure 3**), which supports the ability of ApcI to bind to PBSs and mediate its interaction with PSII (**Figure 5&6**). These observations strongly suggest that ApcI interacts peripherally with PSII at the thylakoid membrane; this explains its accumulation in the soluble cell extract (**Figure 4C**), while absent in isolated PBSs (**Supp. Figure S12**) but present in solubilized thylakoids (**Figure 6**). Our observations lead to a model for the expression and interaction of ApcI with PSII in which, under normal conditions (balanced redox state of the plastoquinone pool), ApcG mediates the PBS-PSII interaction, however under the conditions that reduce the plastoquinone pool, such as red light, ApcG is replaced by ApcI (**Figure 7**).

Both ApcG and ApcI support growth under low light conditions (**Figure 2**). While ApcG is ubiquitous among cyanobacteria, the less frequent occurrence of genes encoding ApcI in cyanobacterial genomes (**Figure 1D**) suggests an auxiliary role in light harvesting, consistent with its expression triggered by light quality changes (**Figure 4**). Interestingly, while both linker proteins do not share sequence homology in their N-terminal and middle regions, they both interact with PSII, suggesting that their interactions occur at different sites of the PSII complex. Further investigation is required to identify the specific subunits

from PSII that interact with either ApcG or ApcI to understand their specific roles in the association of the PBS and PSII under light quality changes.

## Materials and methods

### Bioinformatics and structure prediction

The sequences identified as ApcG in Dominguez-Martin et al. (2022) were truncated to their C-terminal PBS-binding motif (*Synechocystis* sp. PCC 6803, ApcG, *sll1873*, residues 75-121) and used to generate an HMM search model by aligning them with ClustalW 2.1 and standard parameters (Thompson et al., 1994), trimming with trimAl (Capella-Gutiérrez et al., 2009) with parameters "-fasta -gt 0.6 -cons 30 -w 3", and the HMMs were generated using hmmbuild 3.3.2 (http://hmmer.org/) with standard parameters (Potter et al., 2018) against the *Synechocystis* proteome which identified Sll1911 as a positive hit. Then a curated list of cyanobacterial proteomes as described in Dominguez-Martin et al. (2022) containing a full-length ApcE (377 proteomes) was searched with hmmsearch 3.3.2 with parameter "-T 40" (http://hmmer.org/) (Potter et al., 2018) to identify 244 protein homologs of ApcI (Sll1911 in *Synechocystis* sp. PCC 6803) (**Supplementary table S1)**. Cyanobacterial proteomes were further classified into bicylindrical, tricylindrical and pentacylindrical according to the length of their ApcE protein. The structural prediction for ApcI was obtained using AlphaFold prediction (Jumper et al., 2021).

### Cyanobacterial growth conditions

*Synechocystis* sp. PCC 6803 strains were cultivated in BG-11 medium (Rippka et al., 1979), buffered to pH 8 with 10 mM HEPES, at 28°C to 30°C, constant illumination (25-30 µmol photons $m^{-2} \cdot s^{-1}$, white light) and supplemented with 3% $CO_2$ (v/v) with agitation (160 rpm), corresponding to normal conditions. Cultures grown under red light (4 µmol photons $m^{-2} \cdot s^{-1}$) (**Supp. Figure S13**) were cultivated in BG-11 medium as stated above but without $CO_2$ supplementation. Selection of mutant strains was performed on BG-11 plates supplemented with 3 g/L sodium thiosulfate and solidified with 1.2% Difco agar (w/v). The antibiotics chloramphenicol (25 µg/mL), kanamycin (50 µg/mL) and

spectinomycin (20 µg/mL) were supplemented to the selection media when appropriate. In case of DBMIB (dibromothymoquinone) or DMCU (3-(3,4-dichlorophenyl)-1,1-dimethylurea) treatments, cyanobacteria cultures grown under normal conditions ($OD_{720}$ 1-1.5) were supplemented either with 50 µM of DBMIB and incubated under the same conditions for another 6 hours, or with 20 µM DCMU and incubated under red light for 24 hours followed by protein extraction.

Growth curves were recorded in Multi-Cultivator MC-1000-MIX (Photon System Instruments, Czechia) in turbidostat regime ($OD_{720}$ = 0.5 – 0.51, corresponding with ~$10^7$ cells $mL^{-1}$) in BG-11 cultivation medium with $FeCl_3$ as the iron source, 50 µM EDTA (van Alphen et al., 2018) and with 17 mM HEPES buffer (pH ≈ 8). Temperature during all turbidostat cultivations was set to 30 °C. $CO_2$ was supplemented by Gas Mixing System GMS-150 (Photon System Instruments) in final concentration 0.5 % (v/v), flow rate within each 80 mL cultivation tube was set to ~ 40 mL $min^{-1}$. Light was provided by red (R615) and warm white (WW) LEDs of the Multi-Cultivator; intensities were set to 10 – 1000 µE $m^{-2}$ $s^{-1}$. The cultures were kept under each particular condition for at least 24 h. This period was long enough to secure full metabolic acclimation (Rodrigues et al., 2023). Specific growth rates were calculated as described in Espinoza-Corral et al. (2024).

**Photosynthetic parameter measurements**

After cyanobacteria growth stabilization in Multi-Cultivators, sampling was performed to measure rapid light curves in light-acclimated state (AquaPen, Photon System Instruments) from which maximum electron transport rate $ETR_{max}$ and non-photochemical quenching coefficient $q_N$ were derived according to the following equations:

$$Q_Y = \frac{F_{m'} - F_t}{F_{m'}} \quad (1)$$

$$ETR = Q_Y * PAR \quad (2)$$

$$ETR_{max} = ETR * \left(\frac{\alpha}{\alpha+\beta}\right) * \left(\frac{\beta}{\alpha+\beta}\right)^{\frac{\beta}{\alpha}} \quad (3)$$

$$q_N = \frac{F_{m'(max)} - F'_m}{F_{m'(max)} - F_{in}} \quad (4)$$

where $F_m$' and $F_t$ are maximal and steady-state fluorescence in light-acclimated state, respectively, $Q_Y$ is quantum yield of PSII (unitless), PAR is photosynthetically active radiation (units µmol photons $m^{-2}$ $s^{-1}$), ETR is electron transport rate (units electron $m^{-2}$ $s^{-1}$) (Ralph and Gademann, 2005), $ETR_{max}$ is maximum electron transport rate, $F_{m'(max)}$ is maximal steady-state fluorescence throughout all tested light intensities of the rapid light curves, $F_{in}$ is steady-state fluorescence at the onset of the rapid light curves measurement, and $q_N$ is a coefficient of non-photochemical quenching, related to dissipation of the captured light energy into heat. The coefficients α and β are slopes of the rapid light curves related to quantum efficiency of photosynthesis and photoinhibition, respectively, derived from light curves fitting (Platt et al., 1980).

In addition, fast fluorescence induction kinetic curves (OJIP) were measured. After sampling from Multi-Cultivators, the cultures were dark-acclimated for 15-20 min, and the OJIP kinetic was measured in MULTI-COLOR PAM (Walz, Germany) using 625 nm saturation pulse of intensity 2,000 µE $m^{-2}$ $s^{-1}$ and duration 600 ms. The parameter $V_J$, corresponding to the redox state of the plastoquinone pool (Toth et al., 2007; Tsimilli-Michael et al., 2009) was calculated as:

$$V_J = \frac{F_J - F_{in}}{F_m - F_{in}} \quad (5)$$

where $F_J$ is fluorescence at the J-level of the OJIP curve, identified by the use of a second derivation of the fluorescence signal (Akinyemi et al., 2023) around 1 ms, and $F_m$ is maximal fluorescence yield.

**Low-temperature fluorescence and absorption spectroscopy**

Absorption spectra were recorded with a white probe beam and a multichannel CCD spectrometer in a fiber-optical spectrometer as described previously (Rose et al., 2023).

Low temperature absorption spectra were recorded by decreasing the temperature stepwise to maintain cell integrity (**Supp. Figure S14**). Fluorescence spectra (**Supp. Figure S15**) were recorded with a home-built instrument (Gurchiek et al., 2020) employing a broadband LED and a compact double monochromator as an excitation source (2 nm spectral bandpass) and a detection system consisting of a 0.15 m spectrograph (4 nm spectral bandpass) and a back-illuminated CCD detector. Whole-cell samples suspended in a 60/40 (*v/v*) glycerol/BG-11 mixture (Espinoza-Corral et al., 2024) were held in 1 cm path length quartz cuvettes in a sample-in-gas liquid nitrogen cryostat (Oxford Instruments OptistatDN, with a MercuryiTC temperature controller). The absorption and fluorescence instruments were controlled by LabVIEW (National Instruments) programs. The spectra reported here are the average of those from three replicate samples.

**Generation and genotyping of *Synechocystis* strains**

Wild type *Synechocystis* sp. PCC 6803 and Δ*apcG* strains (Espinoza-Corral et al., 2024) were used to generate *apcI* deletion strains. This was done by amplifying 500 bp upstream and downstream of *apcI* locus (*sll1911*) with primers oREC5 and oREC6 (**Supp. Table S2**) and cloning it into pJET1.2 generating plasmid pREC1. The *apcI* was deleted from pREC1 by inverse PCR using primers oREC7 and oREC8 introducing a *SacI* restriction site between the upstream and downstream regions of *apcI*, generating plasmid pREC2. A chloramphenicol resistance cassette as well as regions compatible for conjugation from pRL1075 (Black et al., 1993) were introduced into pREC2 using restriction site *SacI*, generating pREC3. Additionally, a second plasmid was generated for the incorporation of a kanamycin resistance cassette from pRL3313 into pREC2 using restriction site *SacI*, generating pREC8. A Bom site compatible for bacterial conjugation was incorporated into pREC8 using primers oREC48 and oREC49 generating pREC19. Over-expression of ApcI for complementation of mutant strains was obtained by cloning *apcI* gene using oREC14 and oREC15 into pET28a using restriction sites *XhoI* and *NdeI*, generating pREC5 which was used as template to amplify *apcI* with a T7 terminator region using primers oREC11 and oCK10, cloned into pPBSA2K5 (to drive the transcription of *apcI* using *psbA2* promoter, P*psbA2*) (Lagarde et al., 2000) using restriction sites *BamHI*

and *NdeI* generating pREC7. A bom site compatible for conjugation was incorporated into pREC7 using primers oREC25 and oREC26 generating pREC10. Additionally, an *aadA* resistance cassette against spectinomycin was incorporated into pREC10 amplifying *aadA* from pRL3332 using primers oREC46 and oREC47 and restriction digestion using site *BamHI*, generating pREC18. Finally, a C-terminal His tag in *apcI* from pREC18 was removed using primers oREC50 and oREC51, generating pREC32. Wild type and Δ*apcG* strains were transformed by conjugation (Black et al., 1993) for the deletion of *apcI* gene using pREC3 (for generating single mutant Δ*apcI* with chloramphenicol resistance cassette) or pREC19 (transforming Δ*apcG* for the double mutant of Δ*apcG*-Δ*apcI* with chloramphenicol and kanamycin resistance cassettes). Genotyping of strains for *apcI* deletion was performed by extracting gDNA (Billi et al., 1998) and amplifying the wild type gene using oREC16 and oREC17, deletion with chloramphenicol cassette using primers oREC16 and oREC27 and deletion with kanamycin cassette using primers oREC16 and oREC44. Furthermore, the deletion of *apcG* was monitored amplifying *apcG* wild type using oREC12 and oREC13 and deletion with oREC12 and oREC27. Likewise, complementation of the single mutant Δ*apcI* and double mutant Δ*apcG*-Δ*apcI* was performed by conjugation using plasmid pREC32 (with spectinomycin resistance cassette). Genotyping of *apcI* complementation was performed by amplifying a region containing *apcI*, *psbA2* promoter (P*psbA2*) and T7 terminator using primers oREC58 and oCK11 using as template gDNA from cyanobacteria.

**Protein expression and purification from *E. coli***

Expression of ApcI and ApcG was done by transforming BL21 DE3 (Invitrogen, Carlsbad, CA, USA) with the corresponding plasmids. For ApcI expression, the *apcI* gene from *Synechocystis* gDNA was amplified using primers oREC55 and oREC56 and cloned into a linearized pBbE2k vector using primers oCK23 and oCK24 by Gibson assembly (Gibson et al., 2009), generating pREC44 for the expression of ApcI with His-SUMO tag at its N-terminus under the control of tetracycline inducible promoter. In case of ApcG, the wild type *apcG* gene from *Synechocystis* gDNA was amplified with primers oREC59 and oREC60 (incorporating a His tag followed by a TEV site at the N-terminus of ApcG) and cloned by blunt ligation into pSL119 linearized with primers oCK3 and oCK4, resulting

in pREC49. The recombinant ApcI$^{\Delta 74\text{-}128}$-His protein started with sub-cloning *apcI* gene from pREC18 into pET11b using restriction digestion sites *BamHI* and *NdeI* which incorporated the His tag at the C-terminus of ApcI in pREC41. The truncation of ApcI deleting the PBS binding motif was performed by inverse PCR of pREC41 using primers oREC33 and oREC37, generating pREC45. Finally, the construct for His-[TEV]-ApcG expression was sub-cloned from pREC49 into pREC44 using restriction sites *NdeI* and *BamHI* generating pREC52 for the expression of His-[TEV]-ApcG under the control of tetracycline inducible promoter.

Expression of His-SUMO-ApcI was performed by transforming BL21 DE3 with pREC44 and growing 4 liters of culture in luria broth at 37°C and induced when $OD_{600}$ reached ~0.7 with 10 *μ*g/mL anhydrous tetracycline at 25°C overnight. Cells were centrifuged and resuspended in Buffer A (50 mM Tris pH 8, 200 mM NaCl) with protease inhibitor cocktail (Sigma, St. Louis, MO, USA), Dnase I (Sigma) and 50 mM imidazole followed by cell lysis using 2 passes through a cell disruptor (Constant Systems, Aberdeenshire, UK) at 15 kPSI. The soluble protein fraction was obtained by centrifuging the cell lysate for 30 min at 45,000 g and 4°C. The fusion protein His-SUMO-ApcI was purified by loading the cell lysate supernatant to a 5 mL HisTrap HP column (GE Healthcare, Little Chalfont, UK), washed with Buffer A, followed by a 5-column volume (CV) of 90% Buffer A and 10% Buffer B (v/v) (50 mM Tris pH 8, 200 mM NaCl, 500 mM imidazole) and eluted with a 5 CV gradient from 10% to 100% Buffer B (v/v). The purified His-SUMO-ApcI was incubated with ULP enzyme (purified in-home from plasmid pARH236 for the expression of fusion protein His-MBP-ULP) at a 1 to 20 ratio in Buffer A overnight at 4°C followed by a subtractive His trap purification using a 5 mL HisTrap HP column (GE Healthcare, Little Chalfont, UK) (GE Healthcare, Little Chalfont, UK) passing the mixture of His-SUMO-ApcI with ULP through the HisTrap column retaining His-SUMO as well as ULP and collecting the flowthrough containing tagless ApcI. Subsequently, ApcI was concentrated using an Amicon tube (Milipore) with 3 kDa cutoff and loaded onto a size exclusion column Superdex 200 increase 10/300 GL (Cytiva) using Buffer A at 4°C (**Supp. Figure S4A**). Finally, ApcI eluted from size exclusion chromatography at size of 32 kDa (**Supp. Figure S4B**) calculated using gel filtration standard (Bio-Rad, 1511901) (**Supp. Figure S4C**).

Expression of recombinant ApcI$^{\Delta 74\text{-}128}$-His using pREC45 was done by transforming BL21 DE3 and inducing 1 liter of cells at $OD_{600}$ ~0.7 with 1 mM IPTG overnight at 25°C. Cells were pelleted and resuspended in Buffer A (50 mM Tris pH 8, 200 mM NaCl) with protease inhibitor cocktail (Sigma, St. Louis, MO, USA), Dnase I (Sigma) and 50 mM imidazole followed by cell disruption using a French press at 4°C. The soluble fraction was obtained by centrifugation for 30 min at 4°C and 45,000 x *g* and subjected to Histrap purification as described above. The elution from the Histrap column was further loaded onto an anion exchange resin (TOYOPEARL DEAE-650, CV 5 mL) using Buffer A with 20 mM NaCl collecting the flowthrough that contained the purified ApcI$^{\Delta 74\text{-}128}$-His.

Moreover, expression of the recombinant His-[TEV]-ApcG was done by transforming BL21 DE3 with pREC52 and using 1 liter of culture grown in LB at 37°C and induced when reaching $OD_{600}$ ~0.7 with 10 *μ*g/mL anhydrous tetracycline at 25°C overnight. Cells were pelleted and resuspended in Buffer A supplemented with protease inhibitor cocktail (Sigma, St. Louis, MO, USA), Dnase I (Sigma) and 50 mM imidazole followed by cell lysis using 2 passes through a cell disruptor. Cell lysate was centrifuged for 30 min and 45,000 x *g* at 4°C to obtain soluble protein fraction which was loaded onto a 5 mL HisTrap HP column. Elution of His-[TEV]-ApcG from Histrap column was performed as described above. Purified His-[TEV]-ApcG was incubated with TEV protease (purified in-home from plasmid pRK793, Addgene 8827) (Kapust et al., 2001) in Buffer A at a ratio of 1 to 20 at 4°C overnight. The digestion of His-[TEV]-ApcG with TEV protease was subsequently loaded onto a 5 mL HisTrap HP column collecting the flowthrough containing tagless ApcG (**Supp. Figure S4E**) following the same protocol above for ApcI. Finally, ApcG was further purified using cation exchange resin (TOYOPEARL SP-650, CV 5 mL) and performed the chromatography by gravity at 4°C as described in Espinoza-Corral et al. (2024). Protein concentration was measured using the BCA method (Pierce BCA Protein Assay Kit, 23227, Thermo Scientific).

**_Synechocystis_ protein extraction**

Cyanobacteria strains grown under normal conditions or red light were cultivated in 10 mL of BG-11 media in 25 mL flasks with agitation till they reached $OD_{720}$ 0.5-1. Total protein extraction was obtained by centrifuging cyanobacteria cells followed by resuspension in extraction buffer at 4°C (50 mM HEPES pH 7.0, 25 mM $CaCl_2$, 5 mm $MgCl_2$, 10% [v/v] glycerol, and protease inhibitor cocktail). Subsequently, cells were broken by French press, followed by the addition of Triton X-100 1% (v/v) and incubation for 10 min on ice. Cell debris was discarded with 2 min centrifugation at 2,000 x *g* at 4°C. When separating soluble and membrane fractions from cyanobacteria cultures, cell pellets were resuspended in buffer TMK (50 mM Tris pH 7.5, 10 mM $MgCl_2$ and 10 mM KCl) with protease inhibitor cocktail (Sigma, St. Louis, MO, USA). After cell disruption by French press, intact cells were discarded in the pellet by centrifuging the samples for 1 min at 2,000 x *g* and 4°C and the supernatant was further centrifuged for 30 min at 20,000 x *g* and 4°C. Supernatant corresponding to the total soluble protein fraction was rescued and the pellet was resuspended in buffer TMK corresponding to membrane fraction. Protein concentration was measured using the BCA method (Pierce BCA Protein Assay Kit, 23227, Thermo Scientific).

**Immunoblot analysis**

Proteins were separated into SDS-PAGE gels and transferred to a nitrocellulose membrane (Amersham, Protran) followed by blocking with 5% fat-free milk (w/v) in TBS (Tris 20 mM and 150 mM NaCl) at room temperature for 1 hour. Incubation of primary antibodies was done overnight at 4°C in TBS-T (TBS with 0.01% tween-20 [v/v]) (anti-PsbA; AS05 084A, anti-PsaB; AS10 695, anti-APC; AS08 277, anti-RPS; AS08 309, Agrisera). Membranes were washed 3 times with TBS-T for 15 min at room temperature and incubated with secondary polyclonal anti-rabbit antisera HRP for one hour at room temperature (Jackson ImmunoResearch, 111-035-003), followed by 3 additional washes with TBS-T and visualized by enhanced chemiluminescence technique.

Primary antibodies against ApcG and ApcI were raised immunizing rabbits with the purified proteins (**Supp. Figure S4**) (Genscript). Bleedings from rabbits were used in

dilutions of 0.25 mL into 1 mL of TBS-T. Antibodies against OCP were used as described in Wilson et al. (2012).

Membranes were mildly stripped by two washes for 10 min at room temperature with striping buffer (200 mM glycine pH 2.2, 0.01% SDS [w/v] and 0.1% tween-20 [v/v]) followed by two subsequent washes with TBS. Stripped membranes were blocked for one hour at room temperature with 5% fat-free milk (w/v) in TBS before incubating with primary antibodies, as described earlier.

**Pull-down experiments**

Wild type *Synechocystis* cultures of 1 liter grown in BG-11 for 1 week under normal conditions were centrifuged and resuspended in 0.1 M phosphate buffer and pH 7.5 with protease inhibitor cocktail and 50 mM imidazole (Sigma, St. Louis, MO, USA) at 4°C. Cells were broken by French press with 4 passes followed by a first centrifugation of 1 min and 2,000 x *g* to discard intact cells and a second of 30 min and 45,000 x *g* at 4°C. The soluble fraction was rescued, and the membrane fraction was solubilized with 10 mL solubilization buffer (1% dodecyl-beta-d-maltoside [w/v], 750 mM aminocaproic acid, 50 mM Bis-Tris pH 7-, and 50 mM imidazole) followed by an incubation of 30 min on ice. Solubilized membranes (majority thylakoids) were centrifuged for 30 min at 30,000 x *g* and 4°C discarding the pellet (insoluble complexes).

Pull-down experiments were performed using the purified ApcI$^{\Delta 74\text{-}128}$-His pre incubated in NTA nickel beads (0.8 mL CV) with either soluble proteins or solubilized thylakoids. Beads were incubated for 1 hour at 4°C and gentle rotation. Non-interacting proteins were washed off from the beads by centrifuging them for 2 min and 100 x *g* at 4°C followed by 4 washes using 10 CV of either 0.1 M phosphate buffer and pH 7.5 with 50 mM imidazole (when using soluble protein fraction) or solubilization buffer (when using solubilized thylakoids). Elution was obtained by washing the beads with 0.1 M phosphate buffer and pH 7.5 with 200 mM imidazole or solubilized buffer with 200 mM imidazole.

## Separation of protein in first native dimension and second denaturing dimension gels

Samples from pull down experiments using either soluble proteins or solubilized thylakoids as well as solubilized thylakoids from different strains were loaded onto gradient native gels as described by Schagger and Vonjagow (1991). Native gels were run without Coomassie brilliant blue as described by Espinoza-Corral et al. (2024). Second denaturing dimension was utilized to separate the proteins from native gels into 12% SDS-PAGE gels supplemented with 4 M urea. Proteins were visualized using the method described by Blum et al. (1987).

## PBS binding assays

Cyanobacteria PBSs from wild type and mutant strains were isolated following the method described in Espinoza-Corral et al. (2024). Isolated PBSs (obtained from a first sucrose gradient centrifugation) were incubated for 4 hours at 15°C under gentle rotation with either purified ApcI or a mixture of ApcG and ApcI (equimolar ratio, added simultaneously) at a molar concentration of PBS/linker of 0.0015 using 15 pmol of PBS and 10000 pmol linker protein in 0.8 M phosphate buffer (pH 7.5). Samples were loaded onto discontinuous sucrose gradients (corresponding to a second sucrose gradient centrifugation after the initial PBSs isolation) in steps of 1.50, 1.0, 0.75, 0.50, and 0.25 M phases in phosphate buffer (0.8 M, pH 7.5) and centrifuged overnight at 22°C and 25,000 rpm to separate unbound proteins (top of the gradient) from PBS bound proteins (between 0.75 M and 1.00 M sucrose phases). Fractions were recovered from the sucrose gradients (F1 unbound proteins at the top and F2 corresponding to PBS bound proteins) and precipitated by TCA for further analyses.

## Accession numbers

Sequence data from this article can be found in **Supp. Table S1** containing proteins IDs for Uniprot library.

## Software

Figures were produced using Adobe Illustrator CS6 and GraphPad Prism version 6.0 (GraphPad Software, La Jolla, CA, USA; www.graphpad.com). Semiquantitative analyses of western blots were generated using ImageJ (https://imagej.nih.gov). The sequence conservation logo was generated with Weblogo (Crooks et al. 2004) using trimmed sequences by trimAl (Capella-Gutiérrez et al., 2009). AlphaFold2 was used for structure prediction of ApcI (Jumper et al., 2021). Analysis of the rapid light curves and OJIP curves fluorescence data was performed with the use of own-built Python scripts; the tool is available online at https://tools-py.e-cyanobacterium.org.

## Author contributions

R.E.-C. designed and conducted the research, analyzed the data, and wrote the article; T.Z. conducted cyanobacteria growth experiments and photosynthetic parameter measurements and analyzed the data; J.C. analyzed the data; C.L and K.Y conducted low-temperature absorption and fluorescence spectra measurements and W.F.B. analyzed the data; C.A.K. and M.S. designed research, analyzed the data, and wrote the article; all authors provided comments on the manuscript and contributed to experimental design.

## Acknowledgments

Research in the Kerfeld lab was supported by the Office of Science of the U.S. Department of Energy under award number DE-SC0020606. Work in the laboratory of W.F.B. was supported by grant award DE-SC0010847 from the Photosynthetic Systems program of the Office of Basic Energy Sciences, U.S. Department of Energy. T.Z and J.C. were supported by the Ministry of Education, Youth and Sports of CR (grant number LUAUS24149) within the CzeCOS program (grant number LM2018123), and under the OP RDE (grant number CZ.02.1.01/0.0/0.0/16 026/0008413). We thank Dr. Gabrielle Taylor and Dr. Matthew Dwyer for helpful comments on the manuscript, and the anonymous reviewers for valuable comments and suggestions.

## Distribution of materials

The author responsible for distribution of materials integral to the findings presented in this article in accordance with the policy described in the Instructions for Authors (https://academic.oup.com/plcell/pages/General-Instructions) is: Cheryl A. Kerfeld (ckerfeld@lbl.gov)

## REFERENCES


**Adir N, Bar-Zvi S, Harris D** (2020) The amazing phycobilisome. Biochimica Et Biophysica Acta-Bioenergetics **1861**

**Akinyemi OO, Cepl J, Keski-Saari S, Tomaskova I, Stejskal J, Kontunen-Soppela S, Keinanen M** (2023) Derivative-based time-adjusted analysis of diurnal and within-tree variation in the OJIP fluorescence transient of silver birch. Photosynth Res **157:** 133-146

**Beck WF** (2024) Intramolecular charge transfer and the function of vibronic excitons in photosynthetic light harvesting. Photosynth Res **162**, 139–156 (2024)

**Billi D, Caiola MG, Paolozzi L, Ghelardini P** (1998) A method for DNA extraction from the desert cyanobacterium Chroococcidiopsis and its application to identification of ftsZ. Applied and Environmental Microbiology **64:** 4053-4056

**Black TA, Cai YP, Wolk CP** (1993) Spatial Expression and Autoregulation of Hetr, a Gene Involved in the Control of Heterocyst Development in Anabaena (Vol 9, Pg 77, 1993). Molecular Microbiology **10:** 1153-1153

**Blum H, Beier H, Gross HJ** (1987) Improved Silver Staining of Plant-Proteins, Rna and DNA in Polyacrylamide Gels. Electrophoresis **8:** 93-99

**Bryant DA, Canniffe DP** (2018) How nature designs light-harvesting antenna systems: design principles and functional realization in chlorophototrophic prokaryotes. Journal of Physics B-Atomic Molecular and Optical Physics **51**

**Bryant DA, Gisriel CJ** (2024) The structural basis for light harvesting in organisms producing phycobiliproteins. Plant Cell **36:** 4036–4064

**Bryant DA, Guglielmi G, de Marsac NT, Castets A, Cohen-Bazire G** (1979) The structure of cyanobacterial phycobilisomes: a model. Archives of Microbiology **123:** 113–127

**Burnap RL, Troyan T, Sherman LA** (1993) The highly abundant chlorophyll-protein complex of iron-deficient Synechococcus sp. PCC7942 (CP43') is encoded by the isiA gene. Plant Physiol **103:** 893-902

**Calzadilla PI, Kirilovsky D** (2020) Revisiting cyanobacterial state transitions. Photochemical & Photobiological Sciences **19:** 585-603

**Capella-Gutiérrez S, Silla-Martínez JM, Gabaldón T** (2009) trimAl: a tool for automated alignment trimming in large-scale phylogenetic analyses. Bioinformatics **25:** 1972-1973

**Dominguez-Martin MA, Sauer PV, Kirst H, Sutter M, Bina D, Greber BJ, Nogales E, Polivka T, Kerfeld CA** (2022) Structures of a phycobilisome in light-harvesting and photoprotected states. Nature **609:** 835–845

**Dong C, Tang A, Zhao J, Mullineaux CW, Shen G, Bryant DA** (2009) ApcD is necessary for efficient energy transfer from phycobilisomes to photosystem I and helps to prevent photoinhibition in the cyanobacterium Synechococcus sp. PCC 7002. Biochimica et biophysica acta **1787:** 1122-1128

**Ducret A, Müller SA, Goldie KN, Hefti A, Sidler WA, Zuber H, Engel A** (1998) Reconstitution, characterisation and mass analysis of the pentacylindrical allophycocyanin core complex from the cyanobacterium Anabaena sp. PCC 7120. Journal of Molecular Biology **278:** 369-388

**Englund E, Liang F, Lindberg P** (2016) Evaluation of promoters and ribosome binding sites for biotechnological applications in the unicellular cyanobacterium Synechocystis sp. PCC 6803. Sci Rep **6:** 36640

**Espinoza-Corral R, Iwai M, Zavrel T, Lechno-Yossef S, Sutter M, Cerveny J, Niyogi KK, Kerfeld CA** (2024) Phycobilisome protein ApcG interacts with PSII and regulates energy transfer in Synechocystis. Plant physiology **194:** 1383-1396

**Fuente D, Lazar D, Oliver-Villanueva JV, Urchueguia JF** (2021) Reconstruction of the absorption spectrum of Synechocystis sp. PCC 6803 optical mutants from the in vivo signature of individual pigments. Photosynth Res **147:** 75-90

**Gantt E, Edwards MR, Conti SF** (1968) Ultrastructure of Porphyridium Aerugineum a Blue-Green Colored Rhodophytan(1,2,3). J Phycol **4:** 65-71

**Gibson DG, Young L, Chuang RY, Venter JC, Hutchison CA, Smith HO** (2009) Enzymatic assembly of DNA molecules up to several hundred kilobases. Nature Methods **6:** 343-U341

**Gindt YM, Zhou J, Bryant DA, Sauer K** (1992) Core mutations of Synechococcus sp. PCC 7002 phycobilisomes: a spectroscopic study. J Photochem Photobiol B **15:** 75-89

**Gisriel CJ** (2024) Recent structural discoveries of photosystems I and II acclimated to absorb far-red light. Biochim Biophys Acta Bioenerg **1865:** 149032

**Gisriel CJ, Elias E, Shen G, Soulier NT, Flesher DA, Gunner MR, Brudvig GW, Croce R, Bryant DA** (2023a) Helical allophycocyanin nanotubes absorb far-red light in a thermophilic cyanobacterium. Sci Adv **9:** eadg0251

**Gisriel CJ, Ranepura G, Brudvig GW, Gunner MR** (2024) Assignment of chlorophyll d in the Chl(D1) site of the electron transfer chain of far-red light acclimated photosystem II supported by MCCE binding calculations. Biochim Biophys Acta Bioenerg**:** 149496

**Gisriel CJ, Shen G, Flesher DA, Kurashov V, Golbeck JH, Brudvig GW, Amin M, Bryant DA** (2023b) Structure of a dimeric photosystem II complex from a cyanobacterium acclimated to far-red light. J Biol Chem **299:** 102815

**Glauser M, Bryant DA, Frank G, Wehrli E, Rusconi SS, Sidler W, Zuber H** (1992) Phycobilisome Structure in the Cyanobacteria Mastigocladus-Laminosus and Anabaena Sp Pcc-7120. European Journal of Biochemistry **205:** 907-915

**Glazer AN, Williams RC, Yamanaka G, Schachman HK** (1979) Characterization of cyanobacterial phycobilisomes in zwitterionic detergents. Proc Natl Acad Sci U S A **76:** 6162-6166

**Govindjee, Shevela D** (2011) Adventures with cyanobacteria: a personal perspective. Front Plant Sci **2:** 28

**Guikema JA, Sherman LA** (1983) Organization and Function of Chlorophyll in Membranes of Cyanobacteria during Iron Starvation. Plant Physiol **73:** 250-256

**Gurchiek JK, Rose JB, Guberman-Pfeffer MJ, Tilluck RW, Ghosh S, Gascón JA, Beck WF** (2020) Fluorescence Anisotropy Detection of Barrier Crossing and Ultrafast Conformational Dynamics in the S State of β-Carotene. Journal of Physical Chemistry B **124:** 9029-9046

**Herrera-Salgado P, Leyva-Castillo LE, Rios-Castro E, Gomez-Lojero C** (2018) Complementary chromatic and far-red photoacclimations in Synechococcus ATCC 29403 (PCC 7335). I: The phycobilisomes, a proteomic approach. Photosynthesis research **138:** 39-56

**Ho M-Y, Gan F, Shen G, Bryant DA** (2017) Far-red light photoacclimation (FaRLiP) in Synechococcus sp. PCC 7335. II.Characterization of phycobiliproteins produced during acclimation to far-red light. Photosynthesis research **131:** 187-202

**Ho M-Y, Shen G, Canniffe DP, Zhao C, Bryant DA** (2016) Light-dependent chlorophyll f synthase is a highly divergent paralog of PsbA of photosystem II. Science (New York, N Y ) **353**

**Hoper R, Komkova D, Zavrel T, Steuer R** (2024) A quantitative description of light-limited cyanobacterial growth using flux balance analysis. PLoS Comput Biol **20:** e1012280

**Jahn M, Vialas V, Karlsen J, Maddalo G, Edfors F, Forsstrom B, Uhlen M, Kall L, Hudson EP** (2018) Growth of Cyanobacteria Is Constrained by the Abundance of Light and Carbon Assimilation Proteins. Cell Rep **25:** 478-486 e478

**Jiang HW, Wu HY, Wang CH, Yang CH, Ko JT, Ho HC, Tsai MD, Bryant DA, Li FW, Ho MC, Ho MY** (2023) A structure of the relict phycobilisome from a thylakoid-free cyanobacterium. Nat Commun **14:** 8009

**Jumper J, Evans R, Pritzel A, Green T, Figurnov M, Ronneberger O, Tunyasuvunakool K, Bates R, Zidek A, Potapenko A, Bridgland A, Meyer C, Kohl SAA, Ballard AJ, Cowie A, Romera-Paredes B, Nikolov S, Jain R, Adler J, Back T, Petersen S, Reiman D, Clancy E, Zielinski M, Steinegger M, Pacholska M, Berghammer T, Bodenstein S, Silver D, Vinyals O, Senior AW, Kavukcuoglu K, Kohli P, Hassabis D** (2021) Highly accurate protein structure prediction with AlphaFold. Nature **596:** 583-+

**Kapust RB, Tözsér J, Fox JD, Anderson DE, Cherry S, Copeland TD, Waugh DS** (2001) Tobacco etch virus protease:: mechanism of autolysis and rational design

of stable mutants with wild-type catalytic proficiency. Protein Engineering **14:** 993-1000

**Kerfeld CA, Sutter M** (2024) Orange carotenoid proteins: structural understanding of evolution and function. Trends in biochemical sciences **49:** 819-828

**Khorobrykh S, Tsurumaki T, Tanaka K, Tyystjärvi T, Tyystjärvi E** (2020) Measurement of the redox state of the plastoquinone pool in cyanobacteria. Febs Letters **594:** 367-375

**Kirilovsky D, Kerfeld CA** (2016) Cyanobacterial photoprotection by the orange carotenoid protein. Nat Plants **2:** 16180

**Kopf M, Klahn S, Scholz I, Matthiessen JK, Hess WR, Voss B** (2014) Comparative analysis of the primary transcriptome of Synechocystis sp. PCC 6803. DNA Res **21:** 527-539

**Lagarde D, Beuf L, Vermaas M** (2000) Increased production of zeaxanthin and other pigments by application of genetic engineering techniques to Synechocystis sp strain PCC 6803. Applied and Environmental Microbiology **66:** 64-72

**Liu HJ, Zhang H, Niedzwiedzki DM, Prado M, He GN, Gross ML, Blankenship RE** (2013) Phycobilisomes Supply Excitations to Both Photosystems in a Megacomplex in Cyanobacteria. Science **342:** 1104-1107

**Luimstra VM, Schuurmans JM, Hellingwerf KJ, Matthijs HCP, Huisman J** (2020) Blue light induces major changes in the gene expression profile of the cyanobacterium Synechocystis sp. PCC 6803. Physiologia Plantarum **170:** 10-26

**Mao HB, Li GF, Ruan X, Wu QY, Gong YD, Zhang XF, Zhao NM** (2002) The redox state of plastoquinone pool regulates state transitions via cytochrome b6f complex in Synechocystis sp. PCC 6803. FEBS Lett **519:** 82-86

**Nishiyama Y, Allakhverdiev SI, Murata N** (2006) A new paradigm for the action of reactive oxygen species in the photoinhibition of photosystem II. Biochim Biophys Acta **1757:** 742-749

**Platt T, Gallegos CL, Harrison WG** (1980) Photoinhibition of Photosynthesis in Natural Assemblages of Marine-Phytoplankton. Journal of Marine Research **38:** 687-701

**Potter SC, Luciani A, Eddy SR, Park Y, Lopez R, Finn RD** (2018) HMMER web server: 2018 update. Nucleic Acids Res **46:** W200-W204

**Ralph PJ, Gademann R** (2005) Rapid light curves: A powerful tool to assess photosynthetic activity. Aquatic Botany **82:** 222-237

**Rast A, Schaffer M, Albert S, Wan W, Pfeffer S, Beck F, Plitzko JM, Nickelsen J, Engel BD** (2019) Biogenic regions of cyanobacterial thylakoids form contact sites with the plasma membrane. Nature Plants **5:** 436-446

**Rippka R, Deruelles J, Waterbury JB, Herdman M, Stanier RY** (1979) Generic Assignments, Strain Histories and Properties of Pure Cultures of Cyanobacteria. Journal of General Microbiology **111:** 1-61

**Rodrigues JS, Kovacs L, Lukes M, Hoper R, Steuer R, Cerveny J, Lindberg P, Zavrel T** (2023) Characterizing isoprene production in cyanobacteria - Insights into the effects of light, temperature, and isoprene on Synechocystis sp. PCC 6803. Bioresour Technol **380:** 129068

**Rose JB, Gascón JA, Sutter M, Sheppard DI, Kerfeld CA, Beck WF** (2023) Photoactivation of the orange carotenoid protein requires two light-driven reactions

mediated by a metastable monomeric intermediate. Physical Chemistry Chemical Physics **25:** 33000-33012

**Saha R, Liu D, Hoynes-O'Connor A, Liberton M, Yu J, Bhattacharyya-Pakrasi M, Balassy A, Zhang F, Moon TS, Maranas CD, Pakrasi HB** (2016) Diurnal Regulation of Cellular Processes in the Cyanobacterium Synechocystis sp. Strain PCC 6803: Insights from Transcriptomic, Fluxomic, and Physiological Analyses. mBio **7**

**Sanfilippo JE, Garczarek L, Partensky F, Kehoe DM** (2019) Chromatic Acclimation in Cyanobacteria: A Diverse and Widespread Process for Optimizing Photosynthesis. Annu Rev Microbiol **73:** 407-433

**Sauer PV, Cupellini L, Sutter M, Bondanza M, Martin MAD, Kirst H, Bína D, Koh AF, Kotecha A, Greber BJ, Nogales E, Polívka T, Mennucci B, Kerfeld CA** (2024) Structural and quantum chemical basis for OCP-mediated quenching of phycobilisomes. Science Advances **10**

**Schagger H, Vonjagow G** (1991) Blue Native Electrophoresis for Isolation of Membrane-Protein Complexes in Enzymatically Active Form. Analytical Biochemistry **199:** 223-231

**Shimizu S, Ogawa H, Tsuboshita N, Suzuki T, Kato K, Nakajima Y, Dohmae N, Shen JR, Nagao R** (2023) Tight association of CpcL with photosystem I in Anabaena sp. PCC 7120 grown under iron-deficient conditions. Biochim Biophys Acta Bioenerg **1864:** 148993

**Sil S, Tilluck RW, Mohan T M N, Leslie CH, Rose JB, Dominguez-Martin MA, Lou W, Kerfeld CA, Beck WF** (2022) Excitation energy transfer and vibronic coherence in intact phycobilisomes. Nature chemistry **14:** 1286-1294

**Soulier N, Laremore TN, Bryant DA** (2020) Characterization of cyanobacterial allophycocyanins absorbing far-red light. Photosynth Res **145:** 189-207

**Soulier N, Walters K, Laremore TN, Shen G, Golbeck JH, Bryant DA** (2022) Acclimation of the photosynthetic apparatus to low light in a thermophilic Synechococcus sp. strain. Photosynth Res **153:** 21-42

**Srivastava R, Singh N, Kanda T, Yadav S, Yadav S, Atri N** (2024) Cyanobacterial Proteomics: Diversity and Dynamics. Journal of proteome research **23:** 2680-2699

**Tamary E, Kiss V, Nevo R, Adam Z, Bernat G, Rexroth S, Rogner M, Reich Z** (2012) Structural and functional alterations of cyanobacterial phycobilisomes induced by high-light stress. Biochimica et biophysica acta **1817:** 319-327

**Thompson JD, Higgins DG, Gibson TJ** (1994) CLUSTAL W: improving the sensitivity of progressive multiple sequence alignment through sequence weighting, position-specific gap penalties and weight matrix choice. Nucleic Acids Res **22:** 4673-4680

**Toporik H, Li J, Williams D, Chiu P-L, Mazor Y** (2019) The structure of the stress-induced photosystem I-IsiA antenna supercomplex. Nature structural & molecular biology **26:** 443-449

**Toth SZ, Schansker G, Strasser RJ** (2007) A non-invasive assay of the plastoquinone pool redox state based on the OJIP-transient. Photosynth Res **93:** 193-203

**Tsimilli-Michael M, Stamatakis K, Papageorgiou GC** (2009) Dark-to-light transition in Synechococcus sp. PCC 7942 cells studied by fluorescence kinetics assesses plastoquinone redox poise in the dark and photosystem II fluorescence component and dynamics during state 2 to state 1 transition. Photosynth Res **99:** 243-255

**van Alphen P, Najafabadi HA, dos Santos FB, Hellingwerf KJ** (2018) Increasing the Photoautotrophic Growth Rate of Synechocystis sp PCC 6803 by Identifying the Limitations of Its Cultivation. Biotechnology Journal **13**

**Watanabe M, Semchonok DA, Webber-Birungi MT, Ehira S, Kondo K, Narikawa R, Ohmori M, Boekema EJ, Ikeuchi M** (2014) Attachment of phycobilisomes in an antenna-photosystem I supercomplex of cyanobacteria. Proceedings of the National Academy of Sciences of the United States of America **111:** 2512-2517

**Wilson A, Gwizdala M, Mezzetti A, Alexandre M, Kerfeld CA, Kirilovsky D** (2012) The Essential Role of the N-Terminal Domain of the Orange Carotenoid Protein in Cyanobacterial Photoprotection: Importance of a Positive Charge for Phycobilisome Binding. Plant Cell **24:** 1972-1983

**You X, Zhang X, Cheng J, Xiao Y, Ma J, Sun S, Zhang X, Wang HW, Sui SF** (2023) In situ structure of the red algal phycobilisome-PSII-PSI-LHC megacomplex. Nature **616:** 199-206

**Zakar T, Herman E, Vajravel S, Kovacs L, Knoppova J, Komenda J, Domonkos I, Kis M, Gombos Z, Laczko-Dobos H** (2017) Lipid and carotenoid cooperation-driven adaptation to light and temperature stress in Synechocystis sp. PCC6803. Biochim Biophys Acta Bioenerg **1858:** 337-350

**Zavrel T, Faizi M, Loureiro C, Poschmann G, Stuhler K, Sinetova M, Zorina A, Steuer R, Cerveny J** (2019) Quantitative insights into the cyanobacterial cell economy. Elife **8**

**Zavrel T, Segecova A, Kovacs L, Lukes M, Novak Z, Pohland AC, Szabo M, Somogyi B, Prasil O, Cerveny J, Bernat G** (2024) A Comprehensive Study of Light Quality Acclimation in Synechocystis Sp. PCC 6803. Plant Cell Physiol

**Zhang X, Xiao Y, You X, Sun S, Sui SF** (2024) In situ structural determination of cyanobacterial phycobilisome-PSII supercomplex by STAgSPA strategy. Nat Commun **15:** 7201

**Zheng L, Zhang Z, Wang H, Zheng Z, Wang J, Liu H, Chen H, Dong C, Wang G, Weng Y, Gao N, Zhao J** (2023) Cryo-EM and femtosecond spectroscopic studies provide mechanistic insight into the energy transfer in CpcL-phycobilisomes. Nature communications **14:** 3961

**Zheng L, Zheng Z, Li X, Wang G, Zhang K, Wei P, Zhao J, Gao N** (2021) Structural insight into the mechanism of energy transfer in cyanobacterial phycobilisomes. Nature communications **12:** 5497

**Zheng Z, Li X, Wei P, Zhang X, Zhang T, Zhang Z, Dong C, Zhao J** (2025) Molecular glue for phycobilisome attachment to photosystem II in Synechococcus sp. PCC 7002. Proc Natl Acad Sci U S A **122:** e2415222122

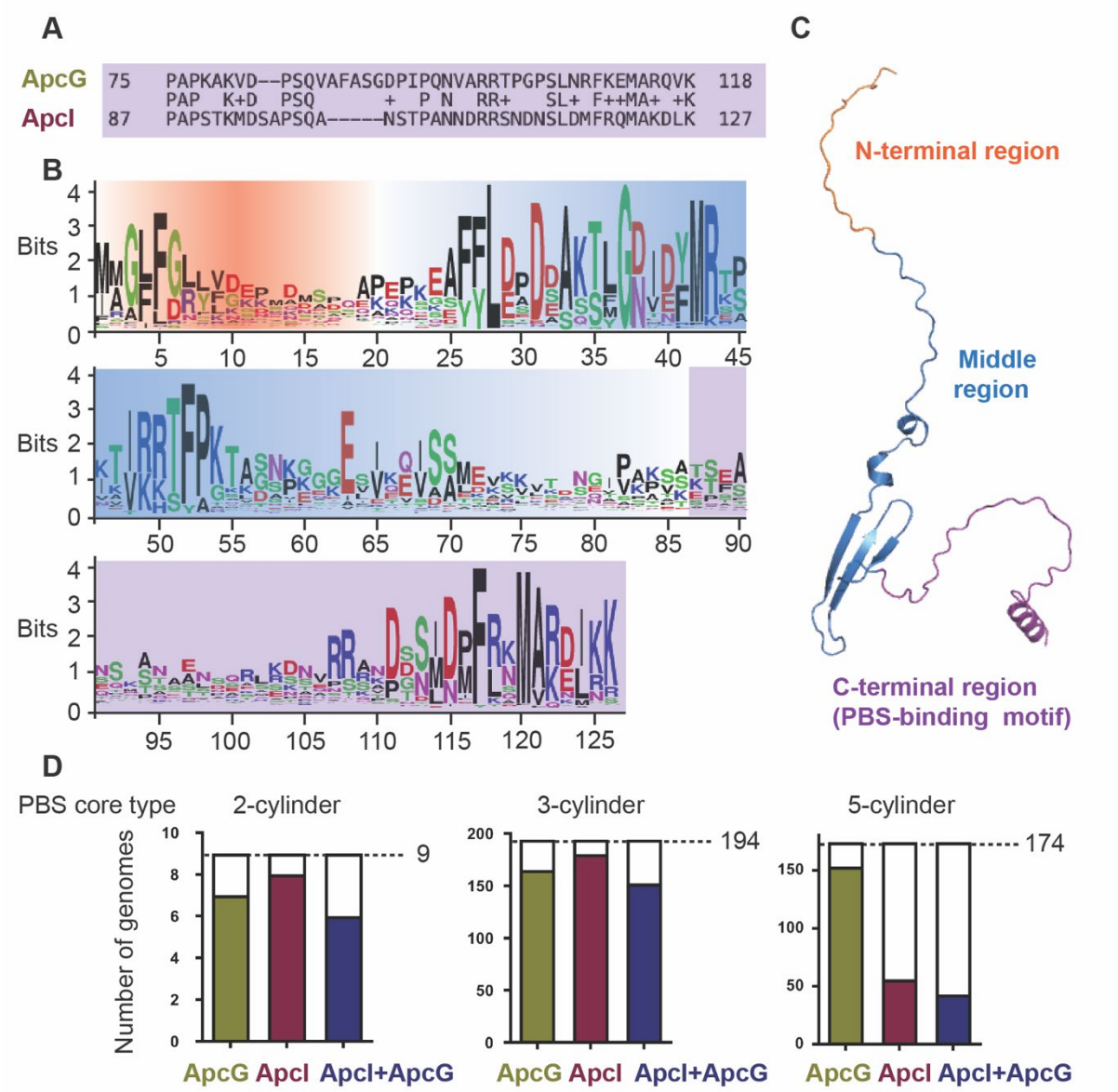


**Figure 1. Sequence and structure overview of ApcI and its occurrence in cyanobacteria.** (**A**) Sequence alignment of the C-terminal regions (PBS-binding motif) of ApcG and ApcI. (**B**) Amino acid sequence conservation logo based on 244 ApcI homologs. The N-terminal region is highlighted in orange; the middle region is highlighted in blue, and the PBS-binding motif is highlighted in purple. (**C**) Alphafold structure prediction of ApcI highlighting the three regions, color coded as in (**B**). (**D**) A total of 377 ApcE-containing genomes were categorized according to their PBS-core type using the domain architecture of the *apcE* gene product as diagnostic. The number of genomes containing a gene encoding for either ApcG or ApcI is shown in bars as well as for the number of genomes with co-occurrence of genes encoding for both ApcG and ApcI.

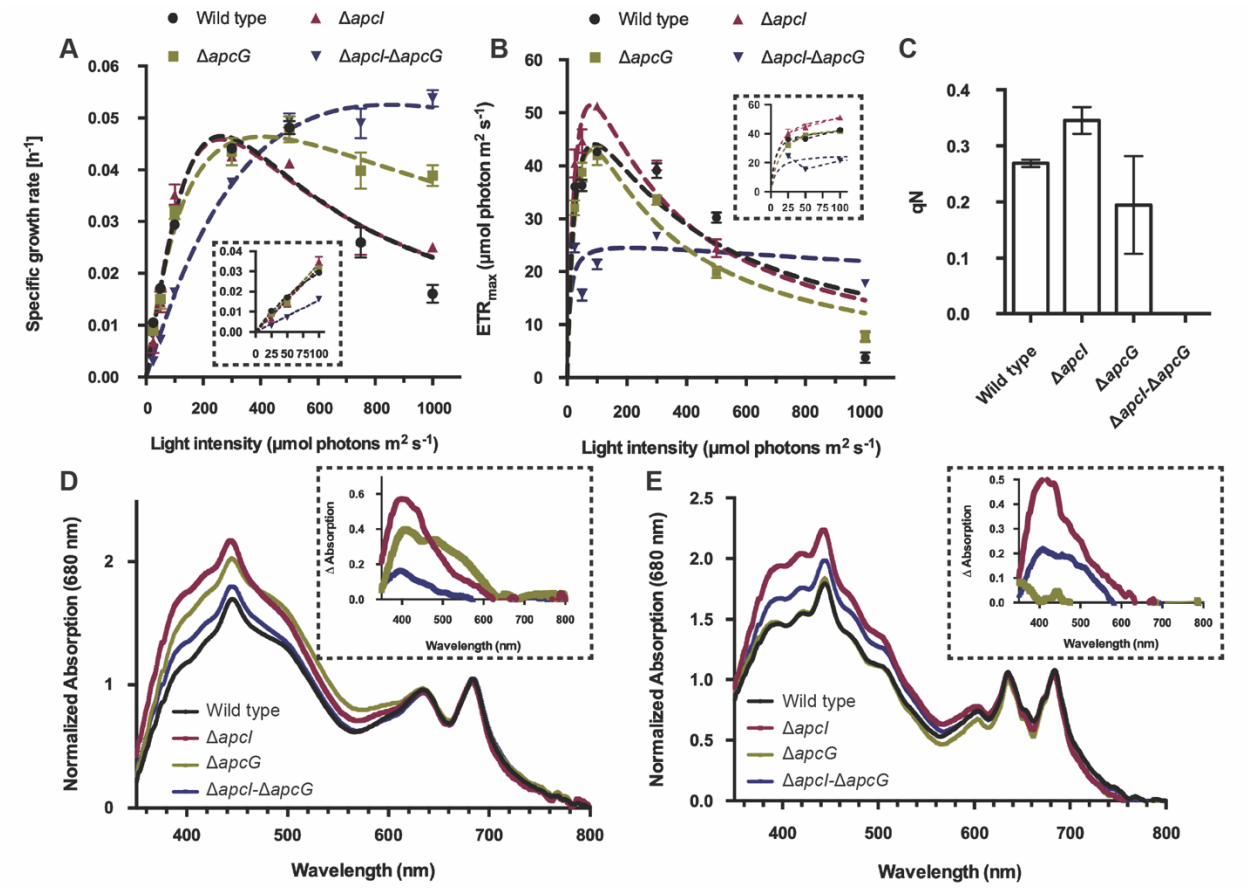


**Figure 2. Physiological characterization of *apcI* strains.** (**A**) Comparison of specific growth rate for Δ*apcG*-Δ*apcI* and double mutant strains with wild type under white light of intensities 25 - 1000 μmol photons $m^{-2} \cdot s^{-1}$. Values correspond to averages of four biological replicates and error bars to SEM (standard error of mean). Fitting curves (Platt et al., 1980) are shown to model the behavior of the strains. Growth rates for the low light intensities are shown within a zoom-in dashed box. (**B**) Maximal electron transport rate ($ETR_{max}$) comparison for single and double mutants with wild type. Values correspond to averages of three biological replicates while error bars correspond to SEM. $ETR_{max}$ for the low light intensities are shown within a zoom-in dashed box. (**C**) Non-photochemical quenching (qN) in strains grown under 1000 μmol photons $m^{-2} \cdot s^{-1}$. Values are presented as relative units (r.u.) (**D**) Whole-cell absorption spectra at room temperature from single, double mutants and wild type strains grown under 25 μmol photons $m^{-2} \cdot s^{-1}$ of white light. Values correspond to normalized signals relative to their absorption at 680 nm. Curves represent averages of three biological replicates. (**E**) Whole-cell absorption spectra measured at 77K for wild type and mutant strains grown under 25 μmol photons $m^{-2} \cdot s^{-1}$ of white light. Values correspond to averages of three biological replicates and are presented as relative units (r.u.). Spectra in (**D**) and (**E**) are shown without error bars for clarity, and insets in (**D**) and (**E**) correspond to average spectra of mutant strains after subtracting the wild type absorption spectrum.

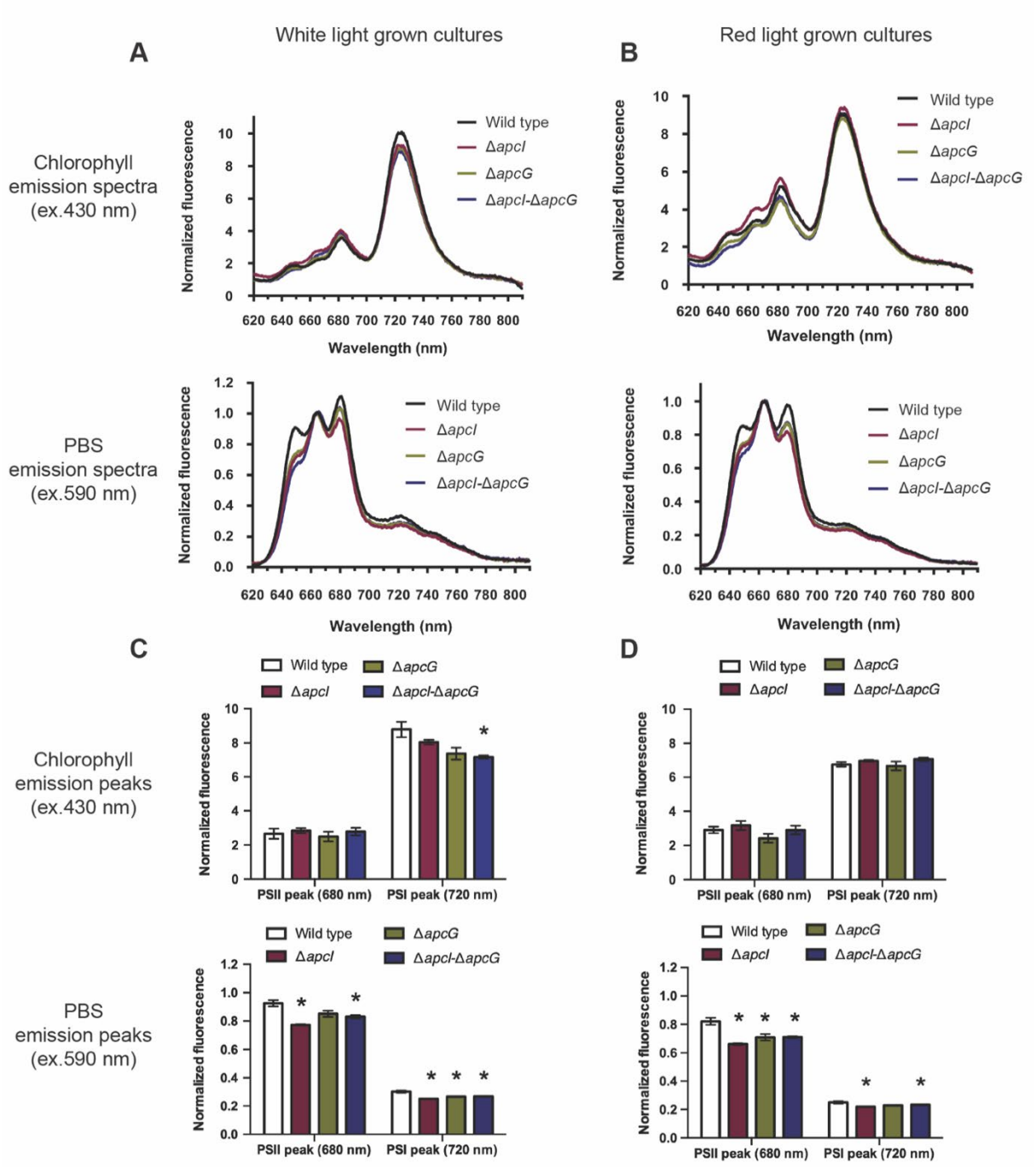


**Figure 3. PBS energy transfer is impaired by the absence of ApcI.** Cultures were grown under white light (25 µmol photons $m^{-2} \cdot s^{-1}$) or red light (4 µmol photons $m^{-2} \cdot s^{-1}$) for 4 days till they reached $OD_{720}$ of 1–1.5 to record their whole-cell fluorescence emission spectra at 77K. Emission spectra of strains grown under white light are shown in panel (**A**), while those grown under red light are shown in (**B**). The spectra correspond to the means of three biological replicates. Chlorophyll emission spectra were normalized by their fluorescence at 800 nm while PBS emission spectra were normalized using the PBS peak at 660 nm. (**C**) Statistical analysis of deconvoluted peaks for PSII (680 nm) and PSI (720 nm) obtained under white light (25 µmol photons $m^{-2} \cdot s^{-1}$) and (**D**) for those under red light (4 µmol photons $m^{-2} \cdot s^{-1}$). Values correspond to mean and error bars to SEM of three biological replicates. An asterisk represents statistical significance ($P < 0.05$) relative to the wild type strain.

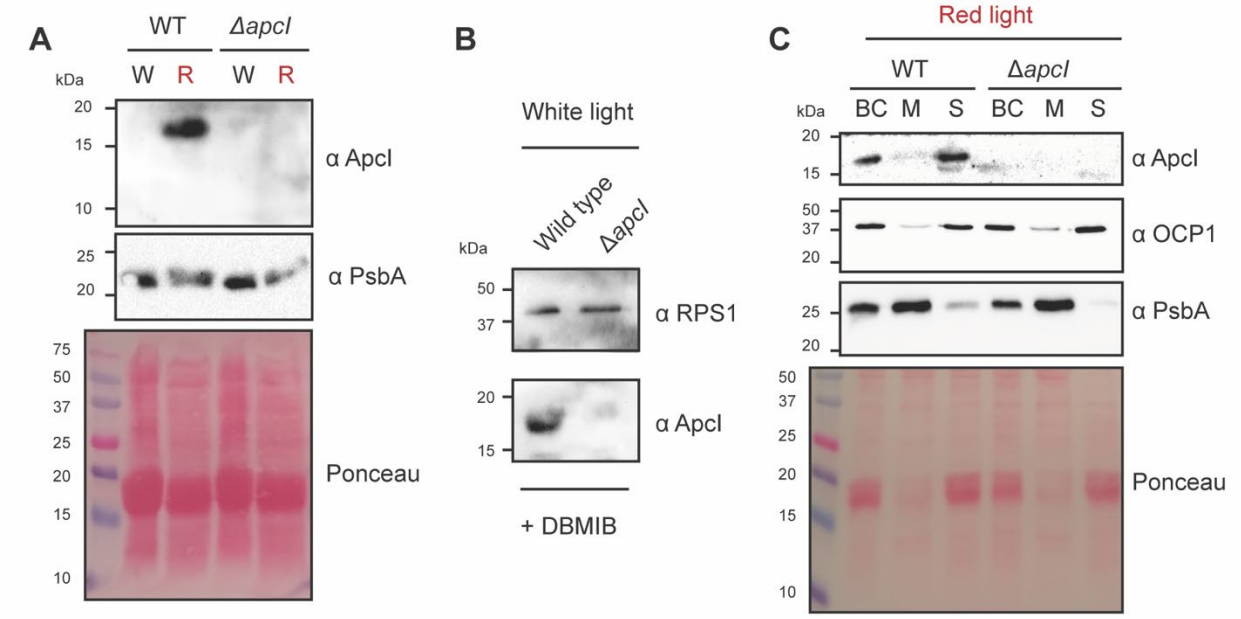


**Figure 4. Expression of ApcI is induced by red light and a highly reduced plastoquinone pool.** Expression of ApcI was monitored using antibodies raised against ApcI full length under different conditions. (**A**) Wild type and *apcI* deletion strains were grown under white light (denoted as W with light intensity of 25 µmol photons $m^{-2} \cdot s^{-1}$) or red light (denoted as R with light intensity of 4 µmol photons $m^{-2} \cdot s^{-1}$) to analyze the presence of AcpI in cell lysates. The subunit PsbA from PSII was used as a control. A total of 50 µg of protein was loaded on each lane. (**B**) Wild type and *apcI* deletion strains were grown under white light in the presence of DBMIB (50 µM) for 6 hours to detect ApcI in cell lysates. Antibodies against the protein RPS1 were used as protein loading control. A total of 25 µg of protein was loaded on each lane. (**C**) Strains were grown under red light for the expression of ApcI. Cell lysates (broken cells: BC) were further separated into membrane (M) and soluble fractions (S) by centrifugation, a total of 25 µg of protein were loaded on each lane. Antibodies against PsbA were used as a marker for the membrane fraction, while antibodies against OCP1 were used as a marker for the soluble fraction. Western blots shown correspond to a representative experiment out of three biological replicates.

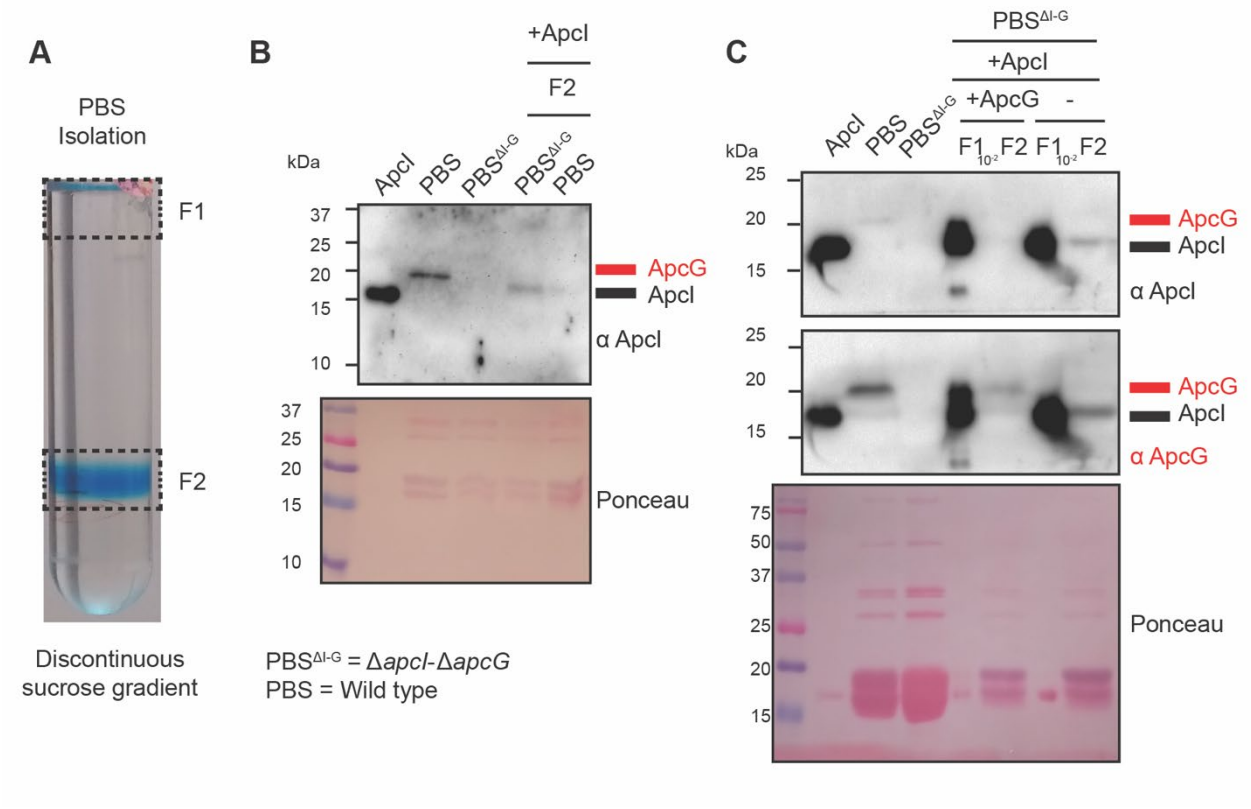


**Figure 5. ApcI and ApcG interchangeable interaction with PBS core.** Isolated PBSs from wild type (denoted as PBS here) and double mutant (Δ*apcI*-Δ*apcG;* denoted as $PBS^{\Delta I\text{-}G}$) strains were used to perform binding assays with purified ApcG and ApcI. (**A**) Discontinuous sucrose gradient profile for the separation of intact PBSs (fraction F2) discarding the excess of unbound protein (F1). (**B**) Wild type and mutant PBSs were used in binding assays with purified ApcI. As a control, the purified protein ApcI was loaded along with isolated PBSs (precipitated by TCA) and fraction F2 (precipitated by TCA). (**C**) Competition binding assay using purified ApcG and ApcI. Fractions were loaded on the gel as described in (**B**). The nitrocellulose membrane was stripped after the detection of ApcI (highlighted in black) followed by incubation with antibodies against ApcG (highlighted in red). Western blots shown correspond to a representative experiment out of three biological replicates. Antibodies against ApcI cross-react with ApcG, nevertheless the two linkers can be distinguished by molecular masses (indicated by colored bars at the right side of the immunoblots).

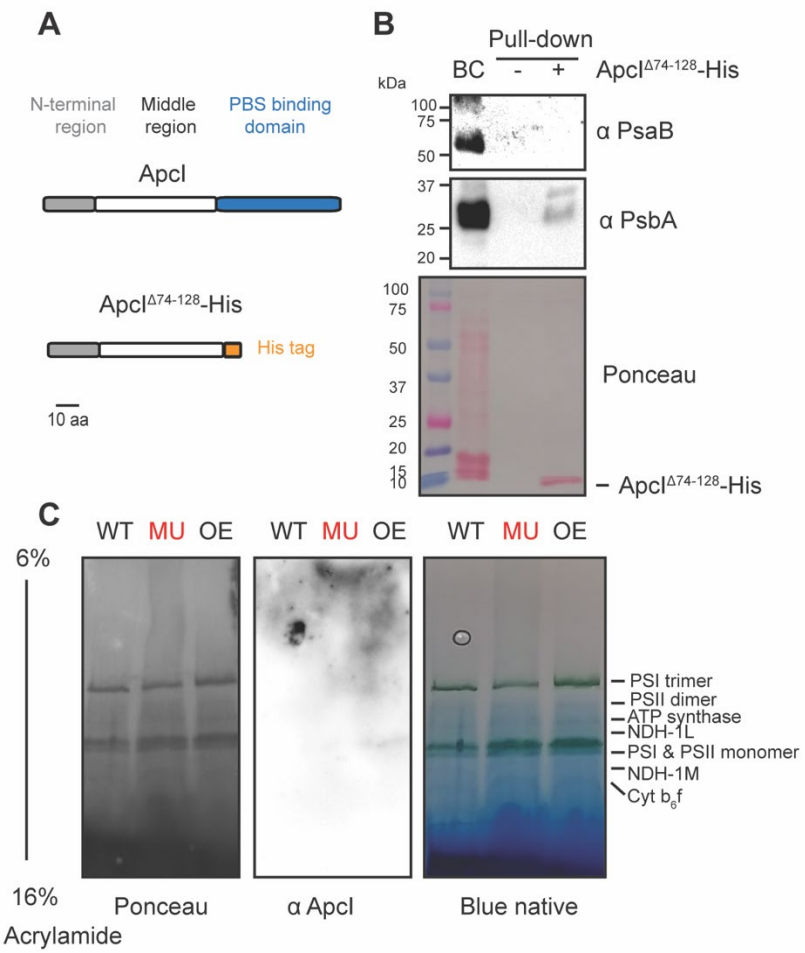


**Figure 6. ApcI interacts with the PSII complex in the thylakoid membrane.** (**A**) Truncated form of ApcI generated to perform pull-down experiments by replacing the PBS binding motif by a C-terminal His tag. (**B**) Pull-down experiments were performed using nickel beads preloaded with ApcI$^{\Delta 74-128}$-His followed by incubation in the presence of *Synechocystis* soluble protein fraction. Antibodies against protein markers were used against PSI (PsaB), PSII (PsbA) and PBS (allophycocyanin; APC). As a control for antibodies, 20 µg of proteins from broken cells (BC) from *Synechocystis* (grown under white light, 25 µmol photons $m^{-2} \cdot s^{-1}$) were used to detect the marker proteins. (**C**) The strains wild type, double mutant (in red as MU; Δ*apcI*-Δ*apcG*) and over-expressor (OE; P*psbA2*::*apcI* in the background of Δ*apcI*-Δ*apcG*) were used to detect ApcI in blots made transferred from blue native gels.

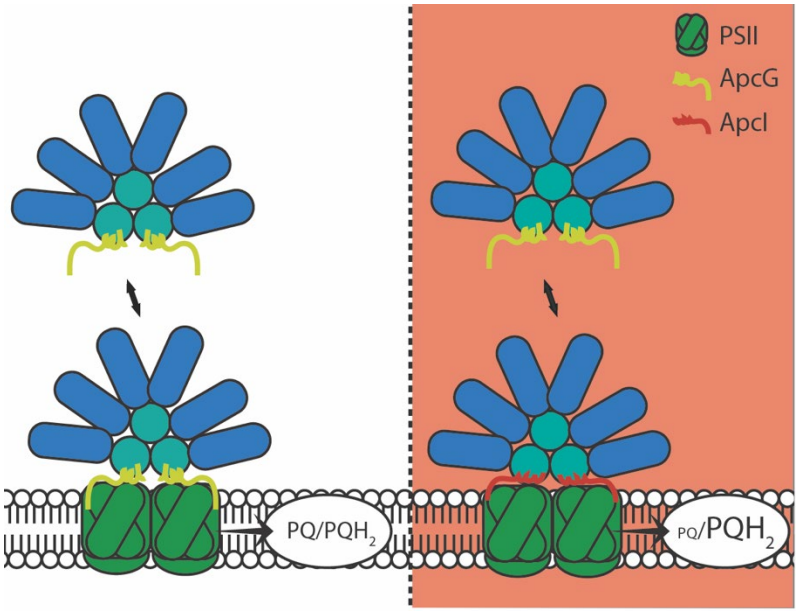


**Figure 7. Model for ApcI expression and interaction with PSII.** Under white light (left panel), the plastoquinone pool is balanced between oxidized and reduced. However, under red light (right panel) the plastoquinone pool becomes more reduced, triggering the expression of ApcI (**Figure 4**) which remains associated with the thylakoid membrane via its N-terminal region (consisting of residues 1-73 which include N-terminal and middle regions) as evident from an ApcI over-expression strain (**Figure 6**). Upon PBS interaction with PSII, ApcG is replaced by ApcI through the C-terminal PBS binding motif of ApcI (**Figure 5**).

## Supplemental figures (S1-15)

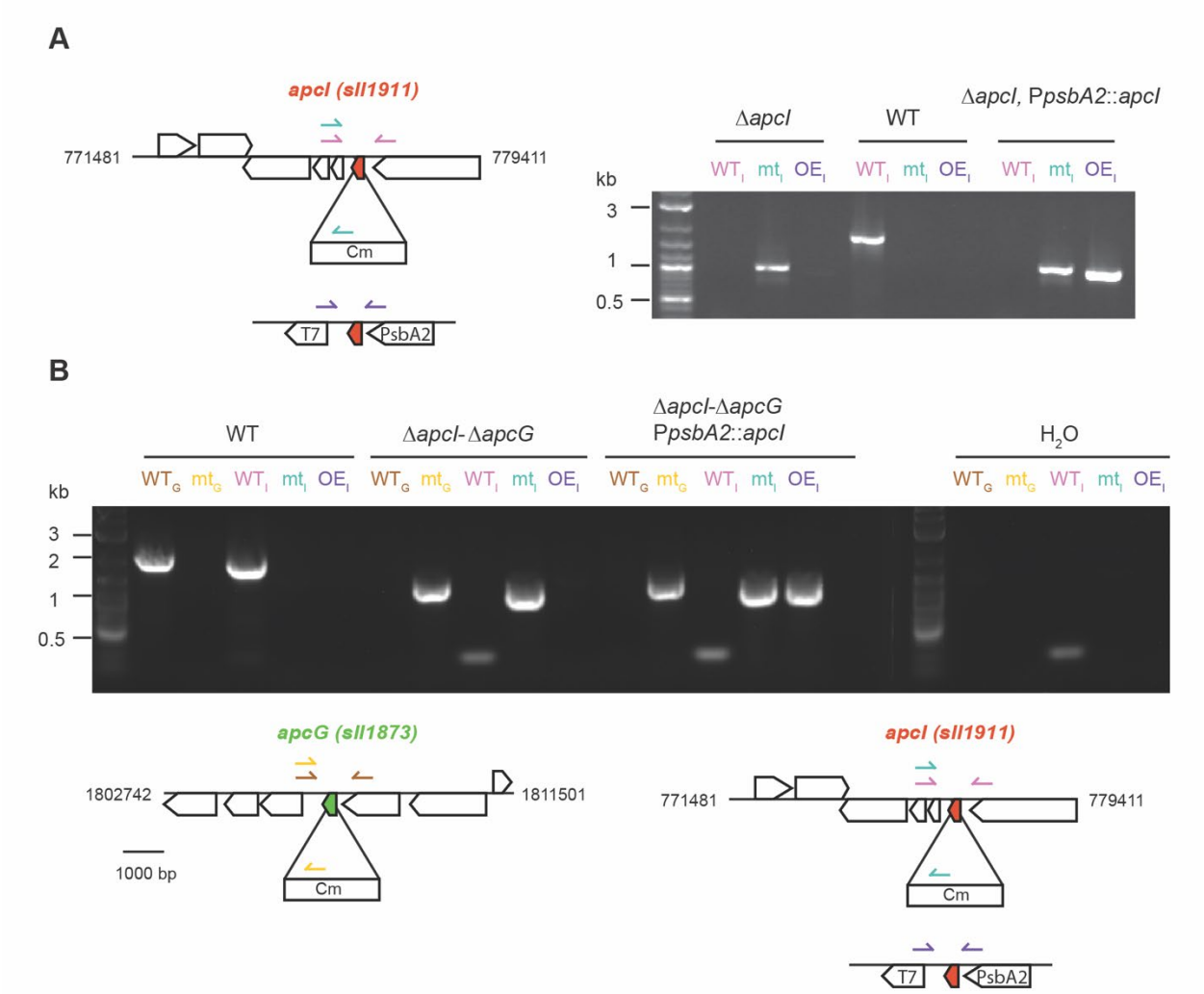


**Supplementary figure S1. Genotyping of cyanobacteria strains.** (**A**) Wild type *Synechocystis* was used to delete the endogenous *apcI* gene by replacing it with a chloramphenicol resistance cassette. The *apcI* deletion strain was used to over-express ApcI under the control of the *psbA2* promoter. (**B**) An *apcG* deletion strain was used to generate a double mutant deleting *apcI* by replacing it with a kanamycin resistance cassette. Additionally, this double mutant strain was used to generate an over-expressor of ApcI under the control of the *psbA2* promoter (P*psbA2*). As a control water was added instead of template for each PCR reaction. Primers used for each PCR reaction are color coded being; $WT_I$ amplification for the wild type gene *apcI*, $MU_I$ mutant amplification for the insertion of either chloramphenicol (Cm) or kanamycin (Kan) cassette replacing the *apcI* gene, $OE_I$ over expression PCR for the replacement of the gene *psbA2* by *apcI* under the control of the promoter P*psbA2*, $WT_G$ amplification for the wild type gene *apcG*, $MU_G$ mutant amplification for the insertion of a chloramphenicol (Cm) cassette replacing the *apcG* gene.

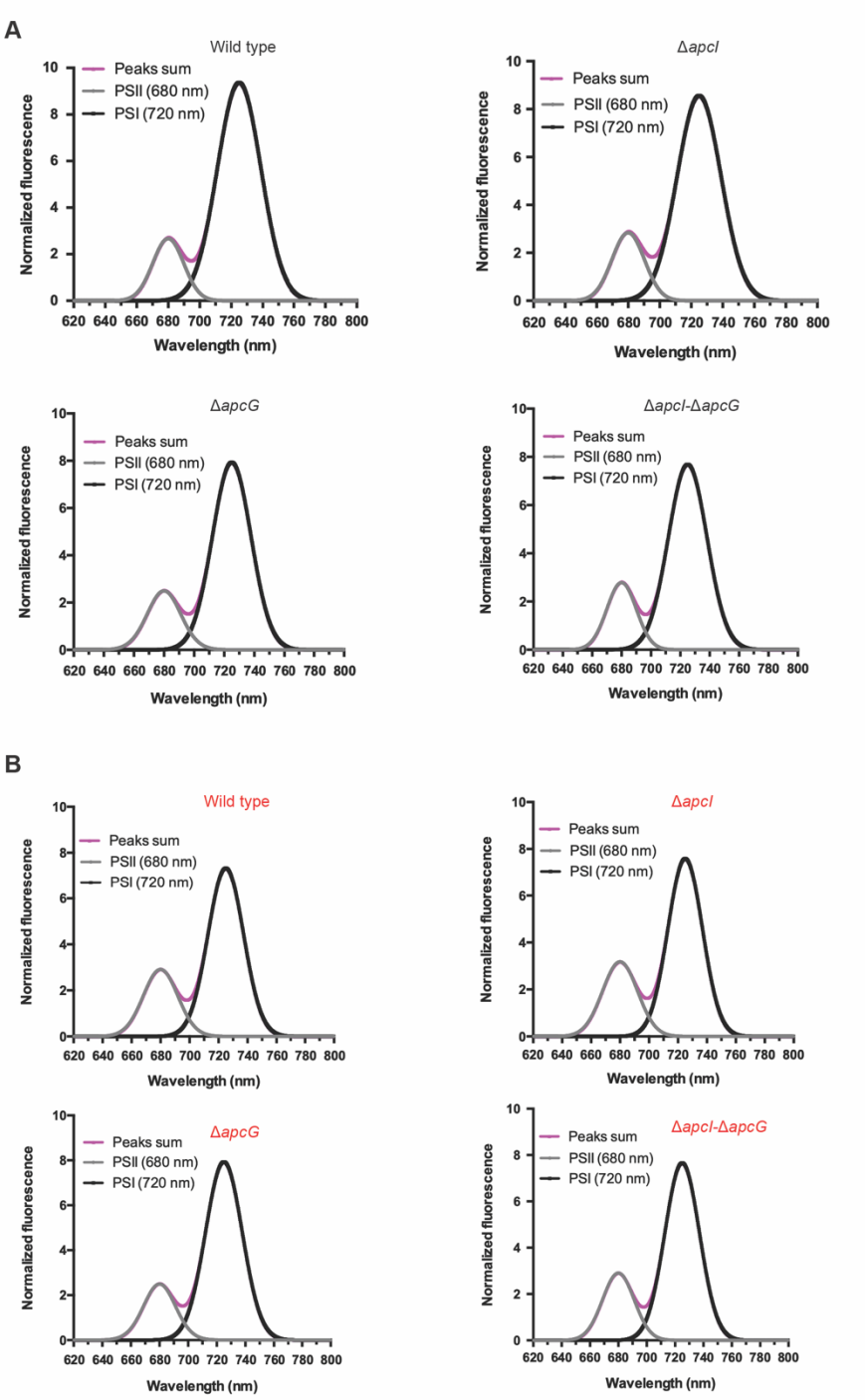


**Supplementary figure S2. Peak deconvolution of chlorophyll low-temperature emission spectra.** Cyanobacterial strains were grown under white light (25 µmol photons $m^{-2} \cdot s^{-1}$) or red light (4 µmol photons $m^{-2} \cdot s^{-1}$), and their whole-cell emission spectra were recorded at 77 K. Peak deconvolution was performed by fitting relative spectra (**Figure 3A** and **B**) to a sum of two Gaussian peaks (PSII at 680 nm and PSI at 720 nm). Gaussian peaks summatory was fitted to relative spectra for the minimum summatory of square error (below 100). Deconvoluted peaks are shown for strains grown under white light (**A**) or red light (**B**). Values represent the mean of three biological replicates.

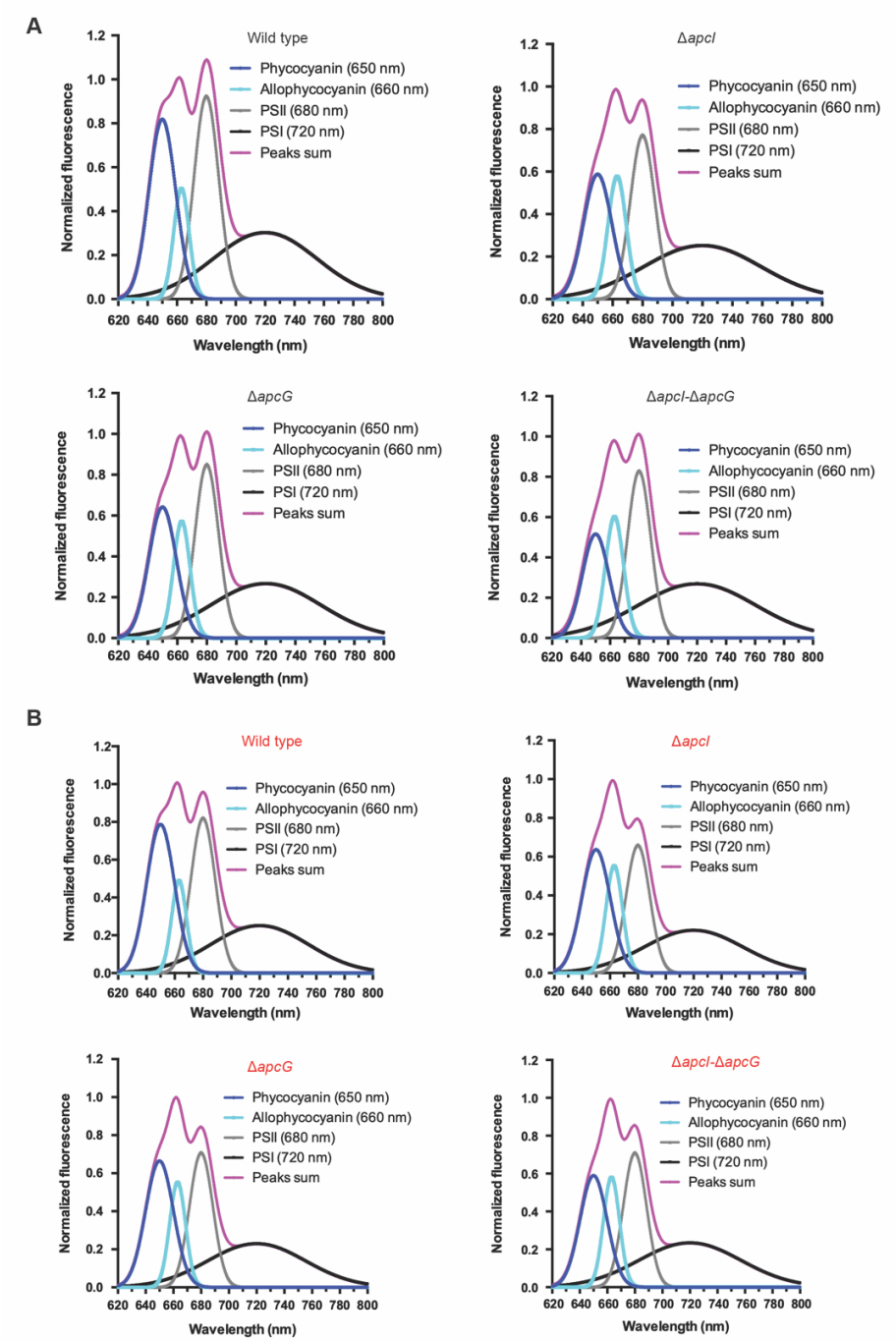


**Supplementary figure S3. Peak deconvolution of PBS low-temperature emission spectra.** Cyanobacterial strains were grown under white light (25 µmol photons $m^{-2} \cdot s^{-1}$) or red light (4 µmol photons $m^{-2} \cdot s^{-1}$), and their whole-cell emission spectra were recorded at 77 K. Peak deconvolution was performed by fitting the relative spectra (**Figure 3A** and **B**) to a sum of four Gaussian peaks (phycocyanin at 650 nm, allophycocyanin at 660 nm, PSII at 680 nm, and PSI at 720 nm). Gaussian peaks summatory was fitted to relative spectra for the minimum summatory of square error (below 100). Deconvoluted peaks are shown for strains grown under white light (**A**) or red light (**B**). Values represent the mean of three biological replicates.

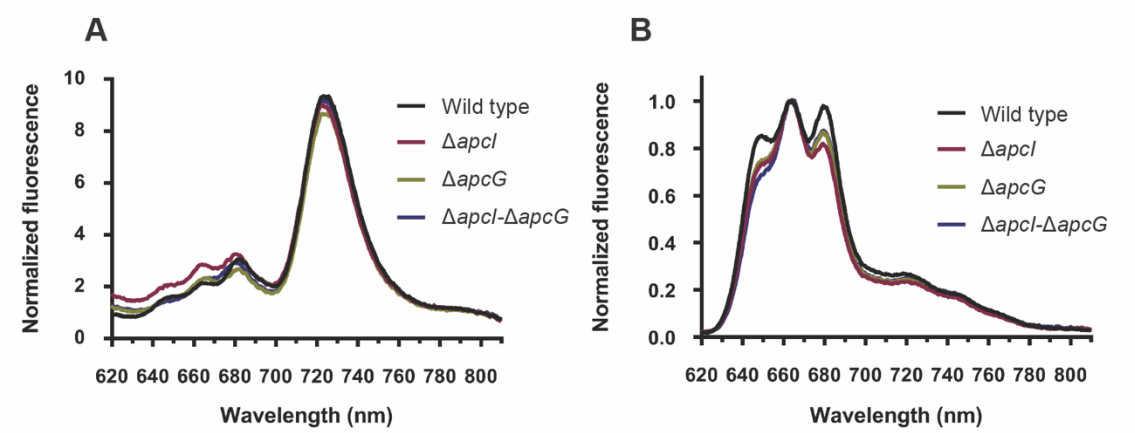


**Supplementary figure S4. Low temperature emission spectra for cultures grown under low white light.** Cyanobacteria strains were grown under low white light (4 µmol photons $m^{-2} \cdot s^{-1}$) without $CO_2$ supplementation, and their whole-cell emission spectra were recorded at 77K. Chlorophyll emission spectra are shown on panel (**A**) (excitation wavelength of 430 nm) and PBS emission spectra on panel (**B**) (excitation wavelength of 590 nm). Values correspond to the means of three biological replicates. Chlorophyll emission spectra were normalized by their fluorescence at 800 nm, while PBS emission spectra were normalized using the peak of PBS at 660 nm.

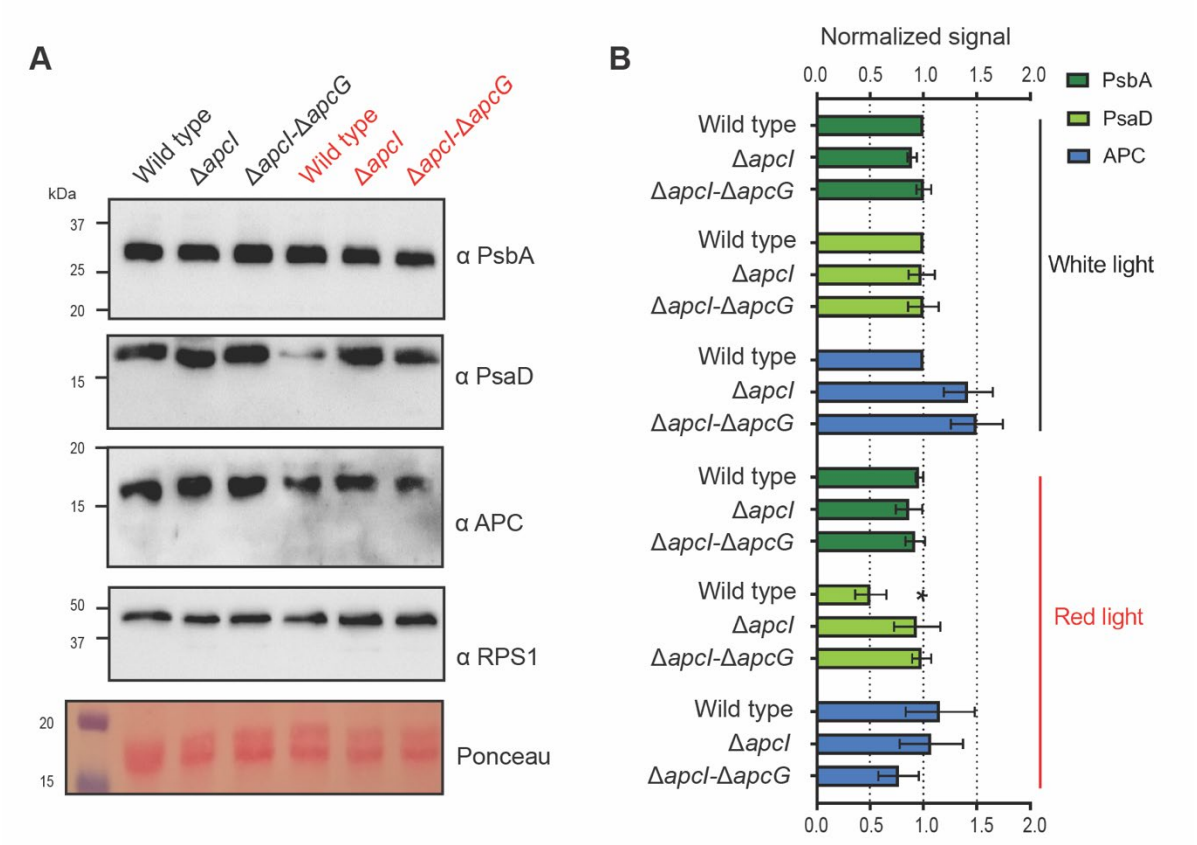


**Supplemental figure S5. Comparison of photosynthetic complexes abundance among cyanobacteria strains.** Wild type, single mutant (Δ*apcI*), and double mutant (Δ*apcI*-Δ*apcG*) strains were grown under white (25 µmol photons $m^{-2} \cdot s^{-1}$) and red light (4 µmol photons $m^{-2} \cdot s^{-1}$) for 4 days to analyze the abundance of photosynthetic complexes from cell lysates. (**A**) Western blot analyses of strains grown under white light (black font) and red light (red font) detecting marker proteins for PSII (PsbA), PSI (PsaD) and PBS (allophycocyanin; APC). Antibodies against RPS1 were used as protein loading control. Images correspond to a representative experiment out of three biological replicates. A total of 25 µg of protein content was loaded on each lane. (**B**) Semi-quantitative analyses of western blot signals for marker proteins. Signals for each of the three biological replicates were normalized according to the signal obtained from wild type grown under white light (first lane of the western blot). Values correspond to mean and error bars to SEM of three biological replicates. An asterisk represents statistical significance at *P* value of 0.05.

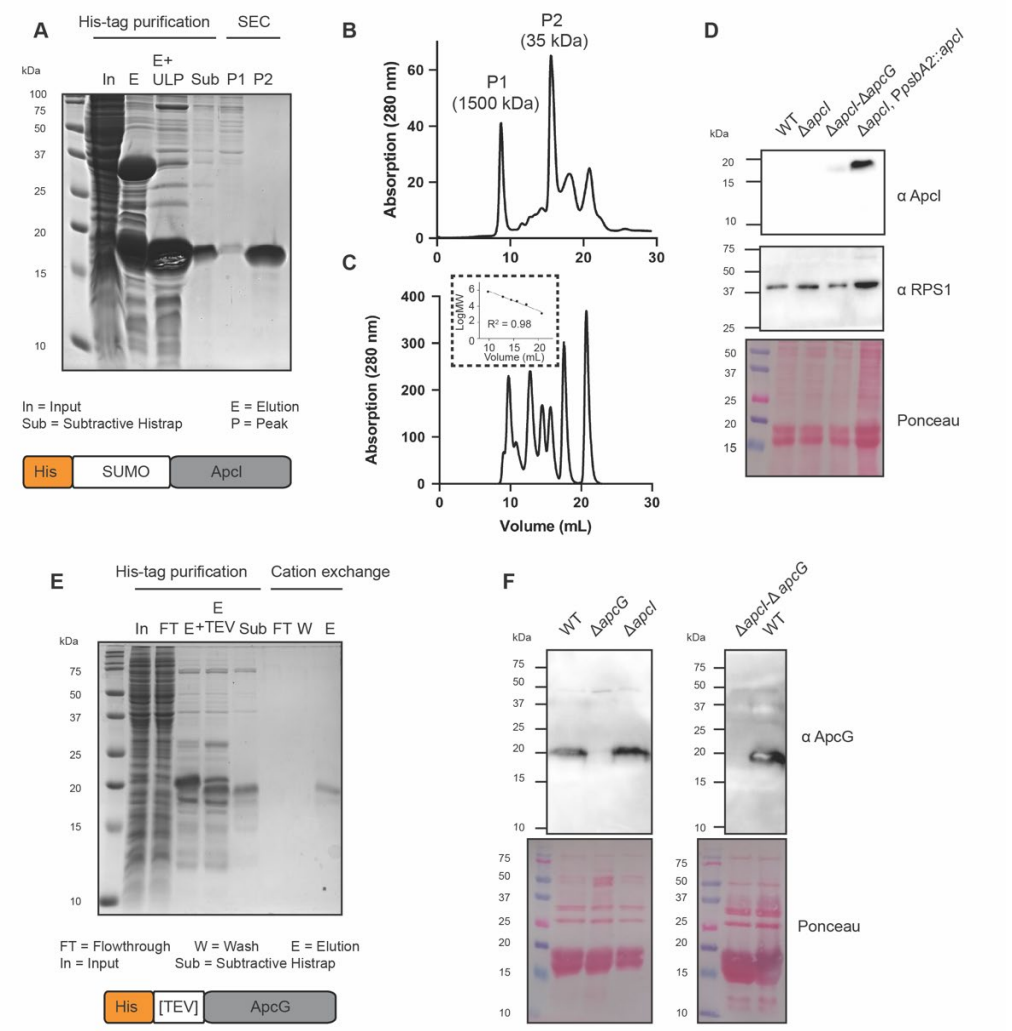


**Supplementary figure S6. Protein purification and antibodies generation.** (**A**) The full length of ApcI was N-terminally fused to His-SUMO for purification by IMAC. Afterwards, the SUMO tag was digested by adding protease His-ULP allowing ApcI to appear in the flowthrough of a subsequent subtractive His tag purification. This fraction was further separated by size exclusion chromatography where the second peak (P2) corresponds to the pure ApcI protein. (**B**) Size exclusion chromatogram for the collection of ApcI after its purification by His tag. (**C**) Standard proteins chromatogram for size exclusion chromatography. In a dashed square it is shown the $R^2$ as well as the standard curve used for calculations. (**D**) Antibodies were generated using the purified protein on **A**. To confirm that the antibodies detect ApcI in cyanobacteria, cell lysates were prepared from wild type (WT) single mutant (Δ*apcI*), double mutant (Δ*apcI*-Δ*apcG*) and ApcI over-expressor strain (Δ*apcI*, P*psbA2::apcI*). Antibodies against RPS1 were used as protein loading control. A total of 50 µg of protein content was loaded on each lane. (**E**) The full length of ApcG was fused to a His tag at its N-terminus with a TEV protease site for the removal of the tag after His tag purification. After purifying the His tagged fusion protein, the His tag was removed by adding protease His-TEV allowing ApcG to appear in the flowthrough of a subsequent subtractive His tag purification. The protein was further purified through a cation exchange gravity column. (**F**) Antibodies were generated using the purified protein on **D**. To confirm that the antibodies detect ApcG, isolated PBSs were obtained from wild type (WT) single mutants for *apcI* and *apcG*, and double mutant (Δ*apcI*-Δ*apcG*). A total of 100 µg of protein content was loaded on each lane after TCA precipitation to remove sucrose from PBSs.

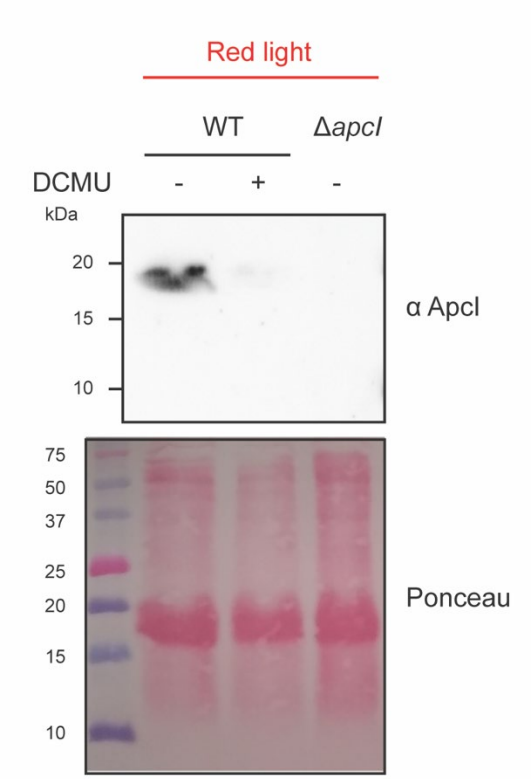


**Supplementary figure S7. An oxidized plastoquinone pool prevents the expression of ApcI under red light illumination.** Wild type and Δ*apcI* strains were grown under red light illumination (4 µmol photons $m^{-2} \cdot s^{-1}$) for one day. Wild type strain was grown in the presence or absence of DCMU 20 µM. Total protein extracts were obtained from cultures and 50 µg of protein were loaded onto a gel to immuno-detect the expression of ApcI using specific antibodies. Figure corresponds representative experiment out of three biological replicates.

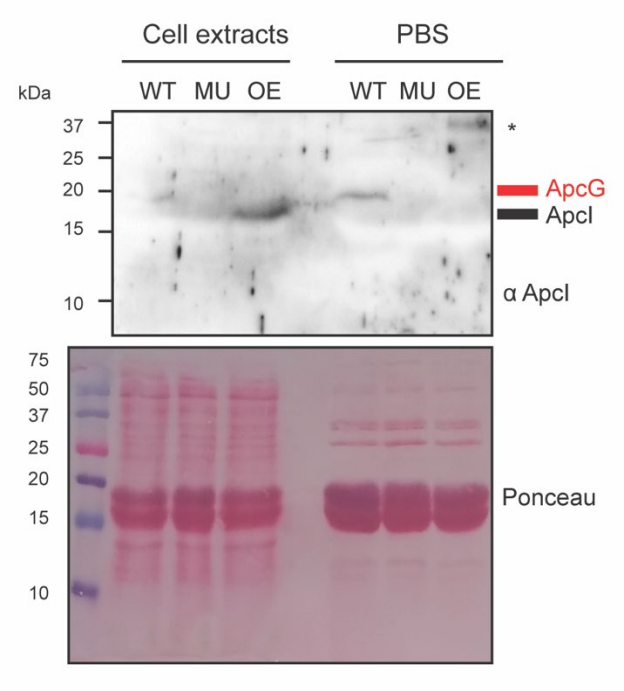


**Supplementary figure S8. Cross reaction of antibodies against ApcI.** Cell extracts and isolated PBSs (precipitated by TCA) from wild type (WT), double mutant (MU; Δ*apcI*-Δ*apcG*) and over-expressor (OE; P*psbA2*::*apcI* in the background of Δ*apcI*-Δ*apcG*) were loaded onto a gel (50 µg of protein content on each lane) to later transfer the proteins to a nitrocellulose membrane and incubate it with antibodies against ApcI. On the right side of the immunoblot in red it is indicated the cross-reaction with ApcG while in black it is shown the size shift for ApcI. Comparison of the wild type (WT) and double mutant (MU; Δ*apcI*-Δ*apcG*) PBSs shows that antibodies against ApcI do recognize ApcG. An asterisk indicates an unspecific band (around 37 kDa) recognized by antibodies against ApcI that was not reproducible in other biological replicates. Strains were grown under white light (25 µmol photons $m^{-2} \cdot s^{-1}$).

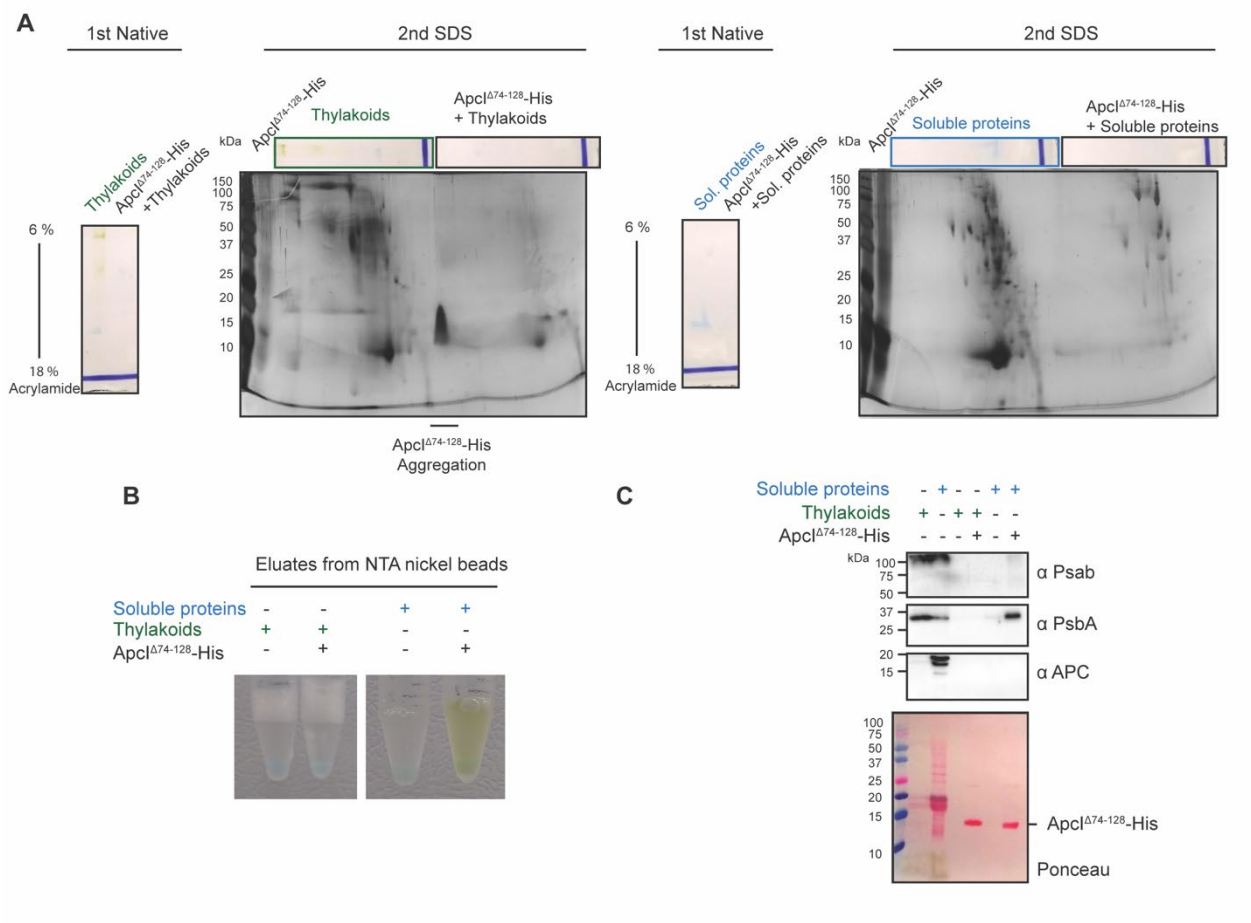


**Supplementary figure S9. Pull-down assays using ApcI truncated version.** A truncated version of ApcI was generated replacing its PBS binding motif by a His tag (ApcI$^{\Delta 74\text{-}128}$-His). After pre-loading nickel beads with ApcI$^{\Delta 74\text{-}128}$-His, fractions of either soluble proteins or solubilized thylakoids were incubated with the nickel beads containing ApcI$^{\Delta 74\text{-}128}$-His. Eluates using 200 mM imidazole were obtained after washing the beads with 50 mM imidazole. As a control, empty nickel beads were incubated with either soluble proteins or solubilized thylakoids. (**A**) First native and second denaturing (SDS) dimensions gels were ran using eluates from pull-down experiments using either soluble proteins or solubilized thylakoids. ApcI$^{\Delta 74\text{-}128}$-His aggregates are shown on the left panel when the protein was incubated with solubilized thylakoids containing 1 % dodecyl-beta-D-maltoside. (**B**) Eluates from control and pre-loaded ApcI$^{\Delta 74\text{-}128}$-His nickel beads incubated with either soluble proteins or solubilized thylakoids. (**C**) Pull-down immunoblots for the detection of marker proteins from PSII (PsbA), PSI (PsaB) and PBS (allophycocyanin, APC) using nickel beads pre-charged with ApcI$^{\Delta 74\text{-}128}$-His.

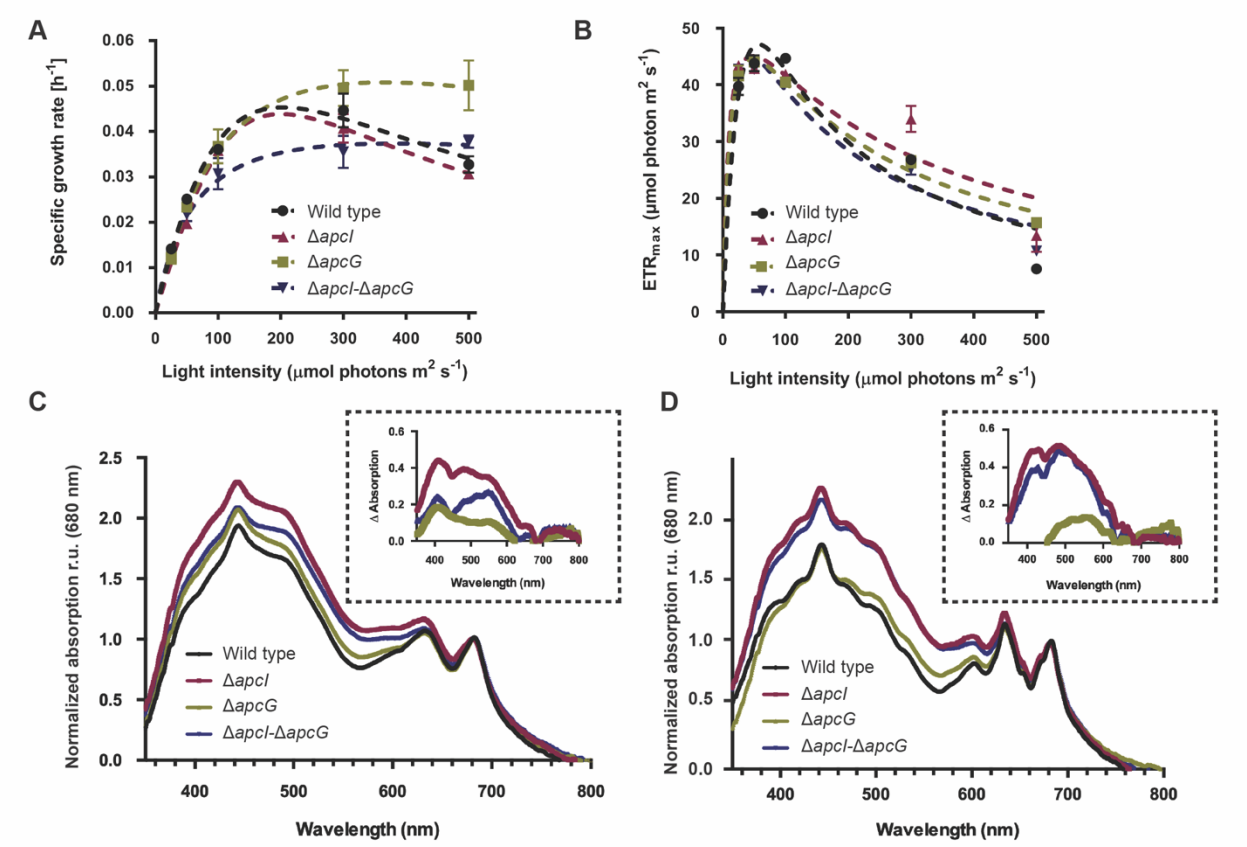


**Supplementary figure S10. Strains phenotypes under increasing red light intensities.** (**A**) wild type, single and double mutant strains for *apcG* and *apcI* were grown under increasing red light intensities and their specific growth measured. Values correspond to averages of four biological replicates and error bars to SEM. (**B**) Maximal electron transport rate of all cyanobacteria strains was measured from cultures grown under different light intensities. Values correspond to average of three biological replicates and error bars to SEM. (**C**) Room temperature whole-cell absorption spectra of cyanobacteria strains grown under red light (4 µmol photons $m^{-2} \cdot s^{-1}$). (**D**) 77K whole-cell absorption spectra under red light (4 µmol photons $m^{-2} \cdot s^{-1}$). Values for (**C**) and (**D**) correspond to averages of three biological replicates presented as relative units (r.u.) and insets to average spectra of mutant strains after subtracting the wild type absorption spectrum.

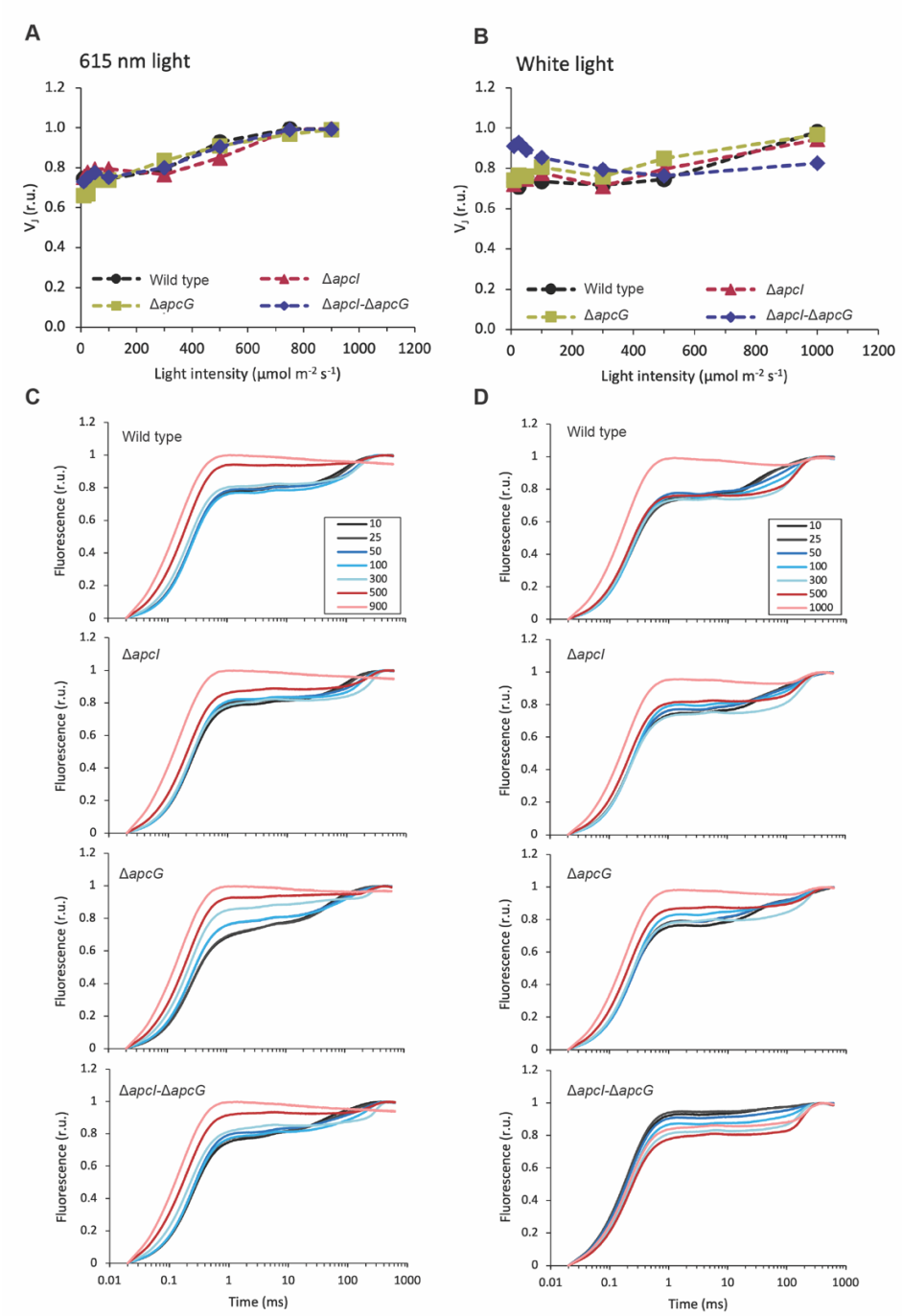


**Supplementary figure S11. Fast fluorescence induction kinetics (OJIP) and the derived parameter VJ as a proxy of the redox state of the plastoquinone pool. The normalized $F_J$ fluorescence**. $V_J$ (**A**, **B**), serving as a proxy for the redox state of the plastoquinone pool (Toth et al., 2007; Tsimilli-Michael et al., 2009) was calculated from fast fluorescence induction curves under red light (**C**) and white light (**D**) according to Eq. (4). The values represent averages (relative units, r.u.) from three biological replicates, error bars represent SD. The OJIP curves, measured after 20 min dark acclimation, were double normalized before plotting and are shown without error bars for clarity. The legends in panels (**C**) and (**D**) represent intensity of red and white light, respectively, under which the strains were cultivated (in units μE $m^{-2}$ $s^{-1}$).

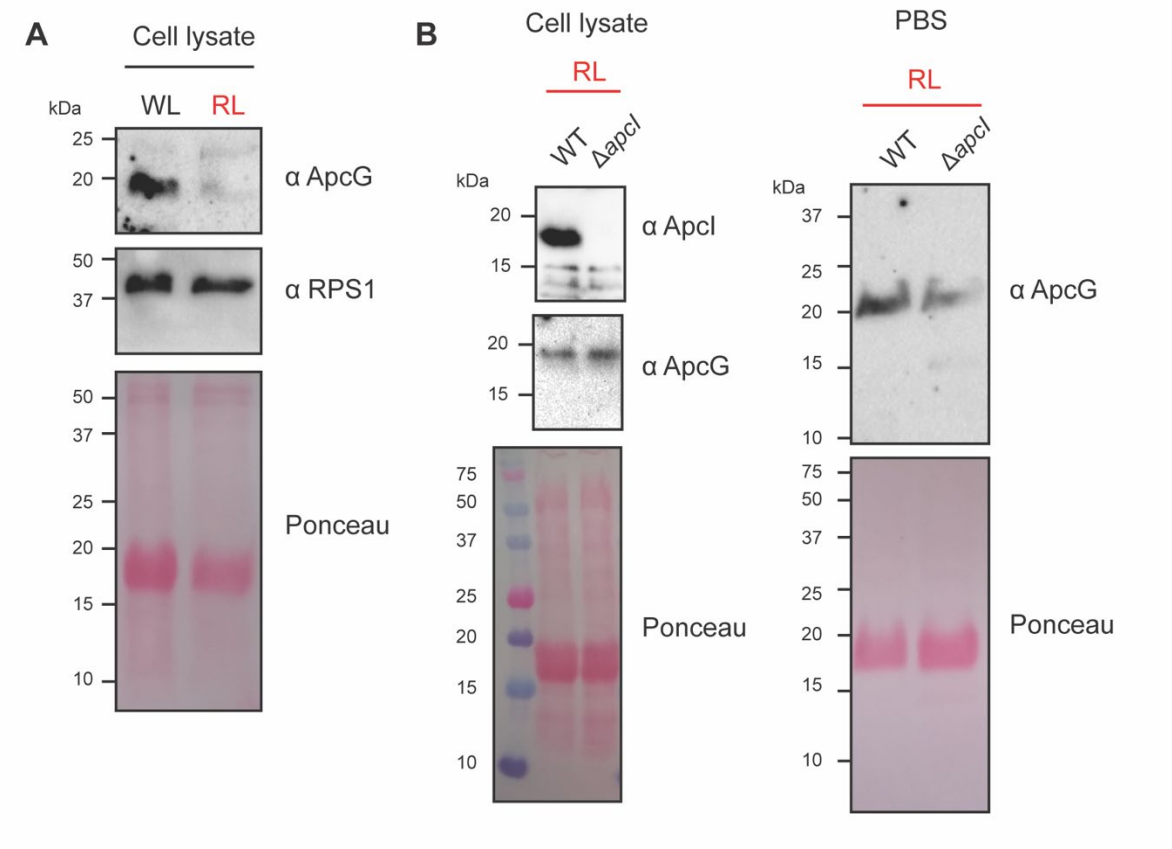


**Supplementary figure S12. ApcG protein levels in isolated PBSs from white and red light grown cultures.** (**A**) Wild type *Synechocystis* cultures were grown to observe the abundance of ApcG in cell lysates from cultures grown for four days under white (WL, 25 µmol photons $m^{-2} \cdot s^{-1}$) or red light (RL, 4 µmol photons $m^{-2} \cdot s^{-1}$). **(B)** Cell lysates and isolated PBSs from wild type and *apcI* deletion strains grown under red light were loaded onto a gel to detect the abundance of ApcG as well as ApcI, however no signal was obtained using antibodies against ApcI in isolated PBS samples. A total of 50 µg of protein content was loaded on each lane for sections (**A**) and (**B**). Immunoblots correspond to a representative experiment out of three biological replicates.

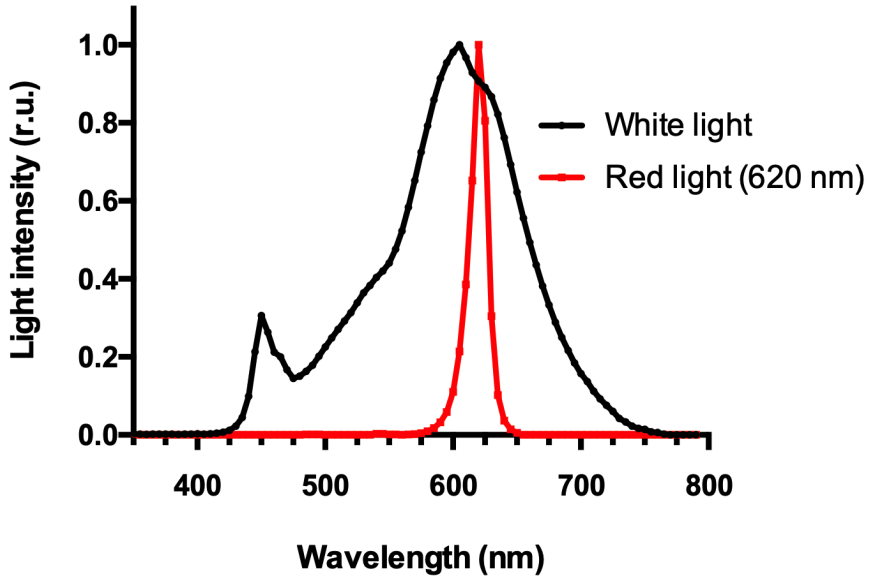


**Supplementary figure S13. Light sources spectra.** Emission spectra of light sources used for growth of cyanobacteria strains. Light intensity is represented as relative units (r.u.).

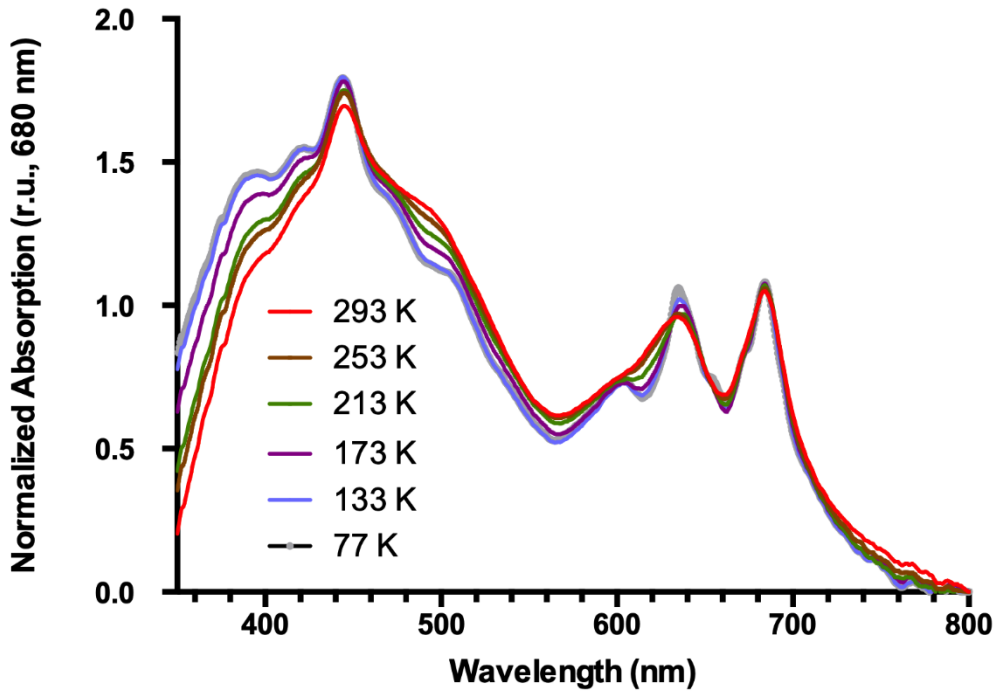


**Supplementary figure S14. Absorption spectra under decreasing temperatures.** Wild type *Synechocystis* cultures were grown under normal conditions (white light) till $OD_{720}$ = 1, and their absorption spectra recorded from 293 K decreasing the temperature of the sample down to 77K. Curves correspond to averages of three biological replicates and are presented as relative units (r.u.).

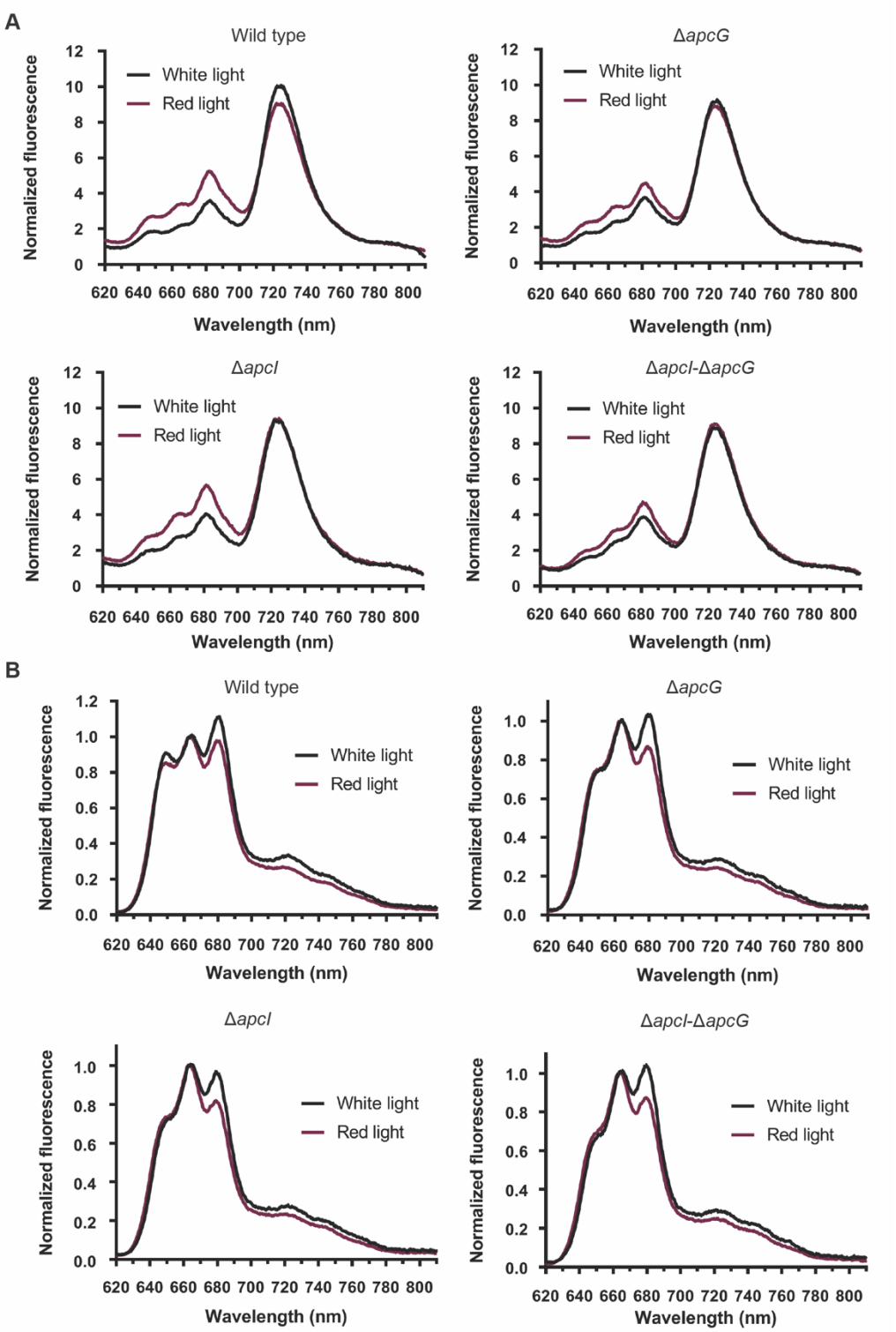


**Supplementary figure S15. Emission spectra of individual strains grown under white and red lights.** (**A**) Chlorophyll emission spectra recorded for all strains under white (25 µmol photons $m^{-2} \cdot s^{-1}$) and red lights (4 µmol photons $m^{-2} \cdot s^{-1}$) by exciting at 430 nm (normalized at 800 nm). (**B**) PBS emission spectra of strains grown under white and red lights (normalized at 660 nm). Values correspond to means of three biological replicates.